Ocean waves in geosciences

part 3: more waves!

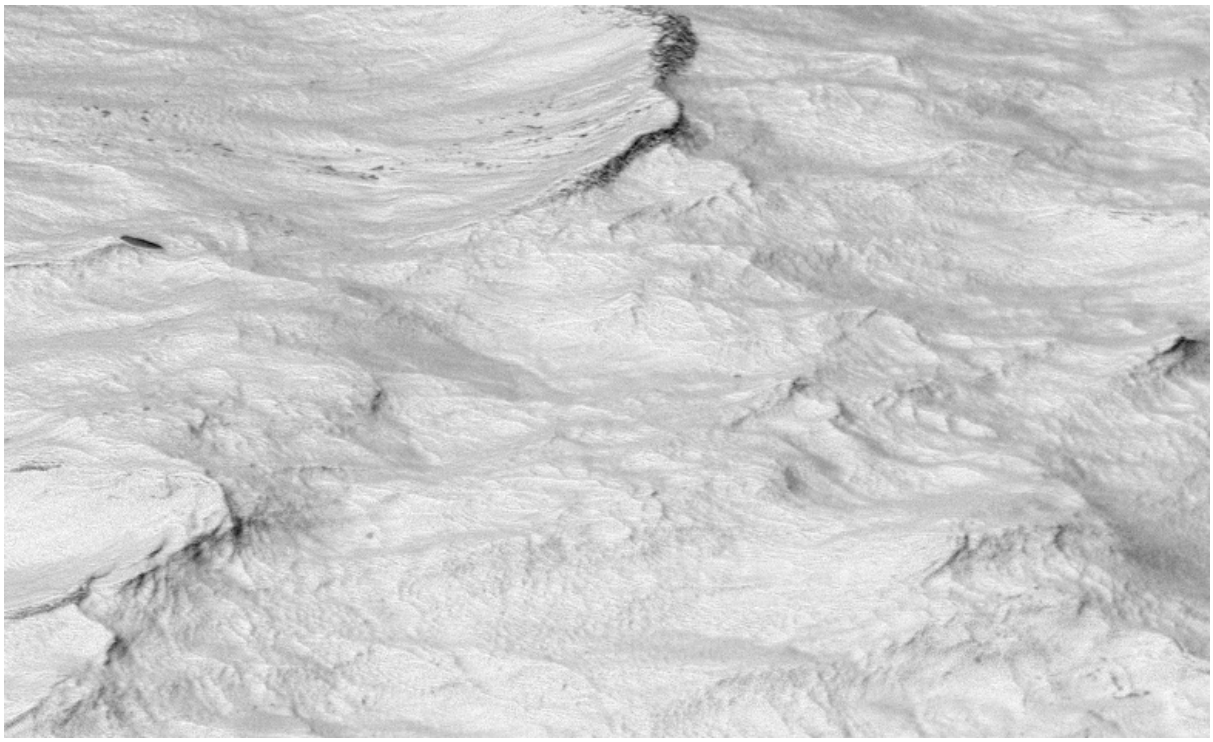

Fabrice Ardhuin,
Laboratoire d'Océanographie Physique et Spatiale, Brest, France
https://github.com/ardhuin/waves_in_geosciences

September 24, 2024

On the cover: a 2 meter wide view of the ocean surface, somewhere near Brest, France, on 3 February 2016. The grey scale represents the Degree of Linear Polarization that is related to the surface slope. This picture Image courtesy of Peter Sutherland. It illustrates that, paraphrasing Richard Feynman "there is plenty of room at the bottom": we are far from understanding all the processes that occur at small scales and create specific patterns on the sea surface. This book touches on some of these, starting with non-linear wave phenomena.

Contents

Foreword: plenty of room at the bottom

This third part details some of the topics briefly discussed in the first two parts, such as wave non-linearities, wave generation by the wind and wave-current interactions. It also adresses other topics that have just been mentionned, such as the generation of seismic and acoustic noise by the waves. As the cover suggests, there is are many detailed processes that we have hardly observed at small scales, where wind waves and current are tightly coupled. These will feedback on larger scales and probably hold the key to the evolution of large scales. For example, wind-wave generation is governed by the details of the air flow over waves which depends on the roughness provided by short gravity-capillary waves. Swell dissipation is presumably governed by air sea friction and the details of the turbulent boundary layer (within a few centimeters from the interface) but these small effects add up over the weeks and thousands of kilometers of swell propagation to transfer energy from the ocean back to the atmosphere. This importance of small scales is also obvious in the observation of the ocean with radars and radiometers. If we are serious about making sense of these observations we can certainly use more of the remote sensing data, beyond the usual parameters, to tell us something about the non-linear properties of the ocean. Satellite altimeters can be used to measure the skewness of the surface elevation that reveal things about short wave - long wave interactions. Other measurements of radar back scatter likewise measure the modulation of short waves: a Modulation Transfer Function (used for CFOSAT or SAR inversion) is a way to get from the measurements to the wave spectrum, it is also a useful scientific measurements of the modulation. There is thus plenty of room for documenting, understanding and building parameterizations of the small scale processes that define the surface geometry and its motions.

Chapter 21

Nonlinear waves over a flat bottom

In this chapter we investigate the consequences of two nonlinear parameters which are the **steepness** $\varepsilon_1 = ka$, and the amplitude normalized by the water depth $\varepsilon_2 = a/D$. The linear theory of Part 1 was obtained in the limit of $\varepsilon_1 = 0$ and $\varepsilon_2 = 0$. After giving the full equations for nonlinear wave motion, this chapter focuses on the properties of monochromatic waves. The next chapter will consider the solution up to second order in ε_1 but extended to a random wave field.

21.1 Dimensional analysis and importance of ε_1 and ε_2

In order to simplify the equations, we will assume here that the mean water level is $\overline{\zeta} = 0$, so that the mean water depth is $D = h$.

The wave equation for irrotational waves includes non-linear terms in addition to the linear term given in chapter 1. These come from the advection in the momentum equation or u^2 and w^2 terms in the Bernoulli equation,

$$\frac{\partial \phi}{\partial t} = -\frac{1}{2}\left[|\boldsymbol{\nabla}\phi|^2 + \left(\frac{\partial \phi}{\partial z}\right)^2\right] - \frac{p}{\rho_w} - gz + C(t), \tag{21.1}$$

and the surface kinematic boundary condition,

$$w = \frac{\partial \phi}{\partial z} = \mathbf{u}\cdot\boldsymbol{\nabla}\zeta + \frac{\partial \zeta}{\partial t} = \boldsymbol{\nabla}\phi\cdot\boldsymbol{\nabla}\zeta + \frac{\partial \zeta}{\partial t} \quad \text{sur} \quad z = \zeta. \tag{21.2}$$

Taking ∂(21.1 at z=ζ)$/\partial t$ +$g\times$(21.2) in order to eliminate the linear ζ terms, gives [1]

$$\frac{\partial^2 \phi}{\partial t^2} + g\frac{\partial \phi}{\partial z} = g\boldsymbol{\nabla}\phi\cdot\boldsymbol{\nabla}\zeta - \frac{1}{2}\frac{\partial \zeta}{\partial t}\frac{\partial^2 \phi}{\partial z \partial t} - \frac{1}{2}\left(\frac{\partial}{\partial t} + \frac{\partial \zeta}{\partial t}\frac{\partial}{\partial z}\right)\left[\boldsymbol{\nabla}\phi\cdot\boldsymbol{\nabla}\phi + \left(\frac{\partial \phi}{\partial z}\right)^2\right] + C'(t), \quad \text{at} \quad z = \zeta. \tag{21.3}$$

We note that the non-linearity comes from the terms on the right hand side but also from the fact that eq. (21.3) is valid at $z = \zeta$, which is unknown. Indeed, a Taylor expansion around $z = 0$ adds many terms, for example

$$\left.\frac{\partial^2 \phi}{\partial t^2}\right|_{z=\zeta} \simeq \frac{\partial^2 \phi}{\partial t^2} + \zeta\frac{\partial^3 \phi}{\partial t^2 \partial z} + \frac{1}{2}\zeta^2\frac{\partial^4 \phi}{\partial t^2 \partial z^2} + ...\Big|_{z=0} \tag{21.4}$$

Before solving this, a question arises: should we really keep all these terms? Do they have the same importance? This is where a dimensional analysis of eq. (21.3) is necessary. This requires to define scales for time and space.

Because we are studying waves, they are naturally characterized by a wavelength $L = 2\pi/k$, a period T, and their amplitude a. Besides, the water depth $D = h + \overline{\zeta}$ comes in the bottom boundary condition. Finally, gravity g is constant and naturally links space and time scale. We can recall the Reech-Froude law for hydrodynamics: if time is multiplied by α, then space is multiplied by α^2, and velocities by α.

We can thus consider that the time scale is fixed by the spatial scale and our problem is thus only a function of the ratios of the different space scales. Since we have a, k et D, we can make two independent

[1] Be careful that, when computing ∂(21.1)$/\partial t$ at $z = \zeta$, you should not forget that ζ is a function of time.

ratios which can be $\varepsilon_1 = ka$, $\varepsilon_2 = a/D$, or $\mu = kD$. The combination of the last two gives the Ursell (1953) number

$$Ur = \varepsilon_2/\mu^2 \tag{21.5}$$

It is common to use ε_1 and Ur. We will see below that a Froude number $\alpha = ga/C^2$, where C is the phase speed, can also have interesting properties (Kirby, 1998).

Let us now look at the different terms in eq. (21.3) following the analysis of Kirby (1998). We take

$$x' = k_0 x, \tag{21.6}$$
$$y' = k_0 y, \tag{21.7}$$
$$t' = k_0 C_0 t, \tag{21.8}$$
$$\zeta' = \zeta/a. \tag{21.9}$$

This gives $\phi' = \phi/\phi_0$ where $\phi_0 = C\alpha/k$ and the Froude number is

$$\alpha = ga/C^2. \tag{21.10}$$

For the vertical coordinate we choose a scale Z, giving $z' = z/Z$. Eq. (21.3) thus becomes

$$\begin{aligned}\frac{\partial^2\phi'}{\partial t'^2} \quad + \quad & \frac{g}{Zk_0^2C_0^2}\frac{\partial\phi'}{\partial z'} = \alpha\boldsymbol{\nabla}\phi'\cdot\boldsymbol{\nabla}\zeta' - \frac{a}{Z}\frac{\partial\zeta'}{\partial t'}\frac{\partial^2\phi'}{\partial z'\partial t'} \\ & - \left(1+\frac{akC}{Z}\frac{\partial\zeta'}{\partial t'}\frac{\partial}{\partial z'}\right)\alpha\left[\boldsymbol{\nabla}\phi'\cdot\frac{\partial\boldsymbol{\nabla}\phi'}{\partial t'} + \frac{1}{k_0^2Z^2}\frac{\partial\phi'}{\partial z'}\frac{\partial^2\phi'}{\partial t'\partial z'}\right] + \frac{C'(t)}{\phi_0k_0^2C_0^2}, \quad \text{at} \quad z' = \frac{a}{Z}\zeta'.\end{aligned} \tag{21.11}$$

If one chooses $Z = 1/k$, then $\alpha = a/Z = \varepsilon_1$ and the linear wave equation only requires $\varepsilon_1 \ll 1$. Choosing instead $Z = D$, will also require $\varepsilon_2 = a/D \ll 1$. Hence the linear wave theory requires both $\varepsilon_1 \ll 1$ and $\varepsilon_2 \ll 1$. It is easy to verify that the solution given in chapter 2 are indeed consistent with these assumptions.

21.2 Finite amplitude solutions

21.2.1 Stokes expansion for weak non-linearity

The common method, introduced by Stokes (1880) is to expand the solution to the nonlinear equations in powers of ε_1, which is most appropriate for deep water waves,

$$\phi = \phi_1 + \phi_2 + \phi_3 + ..., \tag{21.12}$$
$$\zeta = \zeta_1 + \zeta_2 + \zeta_3 + ..., \tag{21.13}$$

in which each term of index n is of order ε^n. Levi-Civita (1925) proved that this expansion was convergent for monochromatic waves. For general random waves, ϕ_1 is the solution to the linear equations, and thus ϕ_1 is a linear sum of monochromatic waves as determined in chapter 2,

$$\phi_1 = \sum_{\mathbf{k},s}\frac{\cosh(kz+kh)}{\cosh(kh)}\Phi^s_{1,\mathbf{k}}\left(\widetilde{t}\right)\mathrm{e}^{\mathrm{i}(\mathbf{k}\cdot\mathbf{x}-s\sigma t)}, \tag{21.14}$$

where σ and $\mathbf{k}$ are related by the linear dispersion relation.

Tke long term evolution of the amplitudes $\Phi^s_{1,\mathbf{k}}$ on time scales $\widetilde{t}$ is not constrained by the linear equations which give constant amplitudes, but this evolution will be part of the solution at higher orders.

When we collect all terms of second order, we have a wave equation for ϕ_2, which is forced by products of ϕ_1 and ζ_1. The full second order solution is given in chapter 22.

We also note that at third order, one obtains a modification of the phase speed. For monochromatic waves in deep water this is (Stokes, 1880)

$$C = gk\left[1+k^2a^2\right]. \tag{21.15}$$

Stokes waves are generally unstable any small perturbation will grow to produce shorter and longer components that will exchange energy with the initial wave. This is known as the instability of Benjamin and Feir (1967). Finite amplitude growth was further analyzed by Chalikov (2007).

21.2.2 Numerical methods for finite amplitude periodic waves

The analytical calculation of the amplitude of different harmonics is becomes very tedious at higher order and has only been completed up to fifth order by De (1955). Beyond fifth order, several method can provide very accurate numerical solutions (Dean, 1965; Dalrymple, 1974; Schwartz, 1974). Such methods have been used by Longuet-Higgins and Fenton (1974) to show that energy and phase speed first grow and then decrease as the wave height increases. Hence, the

Here we use the streamfunction method of Dean, as extended by Dalrymple to allow for a linear current shear such that the velocity potential still satisfies Laplace's equation. This iterative method fits the Fourier amplitudes of the velocity potential to minimise the deviations from a constant pressure along the sea surface. This easily produces the first 100 harmonics for waves that can be really steep, with orbital velocities at the crest $u_{\max}$ up to 98% of the phase speed C, as shown in figure 21.1. We recall that periodic waves break when 100% is reached and no periodic waves can exist with orbital velocities These near-breaking waves are particularly interesting for exploring the kinematics and energetics of breaking waves, although real breaking waves can be very different due to their non-stationary shapes. Cokelet (1977)) introduced the small parameter

$$\epsilon = \left[1 - \frac{q_{\text{crest}}^2 q_{\text{trough}}^2}{C^4}\right]^{1/2} \tag{21.16}$$

with q_{crest} and q_{trough} the orbital velocities at the crest and trough in the frame of reference moving with the wave, so that $q_{\text{crest}} = u_{\max} - C = 0$ in the case of nearly breaking wave. This parameter is clearly between 0 et 1 and allows an expansion in powers of ϵ for nearly breaking waves.

21.2.3 Kinematics of finite amplitude waves

Finite amplitude waves are characterized by flat trough and steeper crests, in particular in shallow water. The orbital velocities are even more asymetric with much larger velocities at the crest than in the troughs. At the limit when $u_{\max}/C = 1$ the surface slope is discontinuous with a 120° angle at the crest.

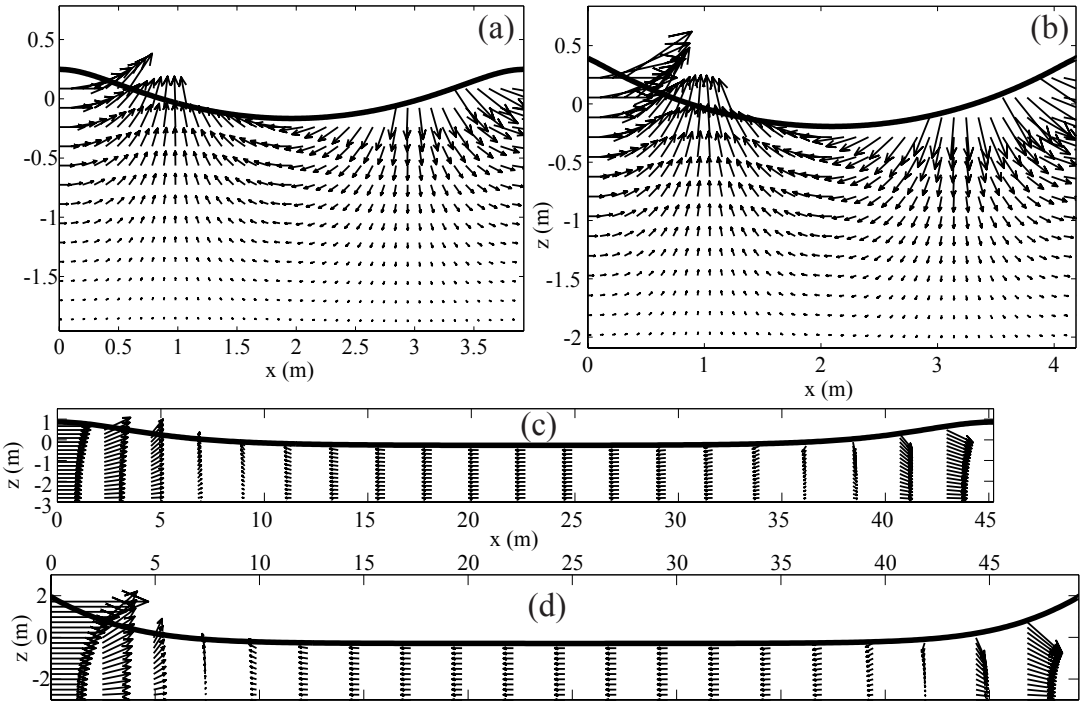

Figure 21.1: Surface elevations and velocity fields at 60th order using Dalrymple (1974)'s numerical method for a water depth of 3 m. (a) and (b) are deep water waves with a period of 1.5 s, so that $kD \simeq 5$. (c) and (d) are shallow water waves of 8 s period. The nonlinearity is intermediate for (a) and (c), with $u_{\max}/C \simeq 0.3$, and extreme in (b) and (d) with $u_{\max}/C \simeq 0.97$.

These nonlinear effects have several consequences. In particular the phase speed, energy and Stokes drift are slightly higher (up to 10% in deep water, much more in shallow water) than predicted by linear theory with the same surface elevation variance (Cokelet, 1977). If accurate estimations of wave kinematics are needed, the linear theory may not be good enough. To know how far the nonlinear solution differ from the linear theory, it is possible to compute numerically the finite amplitude solutions. For example, in the shallow water limit, the surface Stokes drift can exceed several times the linear value (Ardhuin et al., 2008).

21.2.4 Integral properties

The properties of periodic finite amplitude waves over a flat bottom still follow some exact relations. Here we reproduce the results of (Cokelet, 1977). For any water level z_0 below the wave troughs (i.e. such that $-h < z_0 < \min(\zeta)$) we may define,

$$\mathcal{M} = \frac{1}{L}\int_0^L \rho_w \zeta \mathrm{d}x = \rho_w \overline{\zeta}, \tag{21.17}$$

$$\mathcal{C} = \frac{1}{L}\int_0^L \rho_w u(x,z_0)\mathrm{d}x = \rho_w \overline{u}, \tag{21.18}$$

$$M^w = \overline{\int_{-h}^{\zeta} \rho_w u \mathrm{d}z}, \tag{21.19}$$

$$E_c = \frac{1}{2}\overline{\int_{-h}^{\zeta} \rho_w \left(u^2+w^2\right)\mathrm{d}z}, \tag{21.20}$$

$$E_p = \overline{\int_{\overline{\zeta}}^{\zeta} \rho_w g z \mathrm{d}z}, \tag{21.21}$$

$$S_{xx} = \overline{\int_{-h}^{\zeta} \left(p+\rho_w u^2\right)\mathrm{d}z} - \overline{\int_{-h}^{\zeta} p^H \mathrm{d}z} = \overline{\int_{-h}^{\zeta} \left(p+\rho_w u^2\right)\mathrm{d}z} - \frac{1}{2}\rho_w g D^2, \tag{21.22}$$

$$F = \overline{\int_{-h}^{\zeta} \left[p + \frac{1}{2}\rho_w\left(u^2+w^2\right) + \rho_w g\left(z -_z eta\right)\right] u \mathrm{d}z}, \tag{21.23}$$

$$\overline{u_b^2} = \frac{1}{L}\int_0^L u^2\left(x,-h,t\right)\mathrm{d}x. \tag{21.24}$$

In the frame of reference moving at the phase speed, the following three quantities are are independent of the horizontal position x. These are the mass flux per unit crest length,

$$-Q = \int_{-h}^{\zeta} \rho_w \left(u-C\right)\mathrm{d}z = -\rho_w C d. \tag{21.25}$$

the dynamic pressure

$$R = \frac{p}{\rho_w g} + \frac{1}{2g}\left[\left(u-C\right)^2 + w^2\right] + \left(z+h\right), \tag{21.26}$$

and the momentum flux per unit crest length

$$S = \int_{-h}^{\zeta} \left[p + \left(u-C\right)^2\right]\mathrm{d}z. \tag{21.27}$$

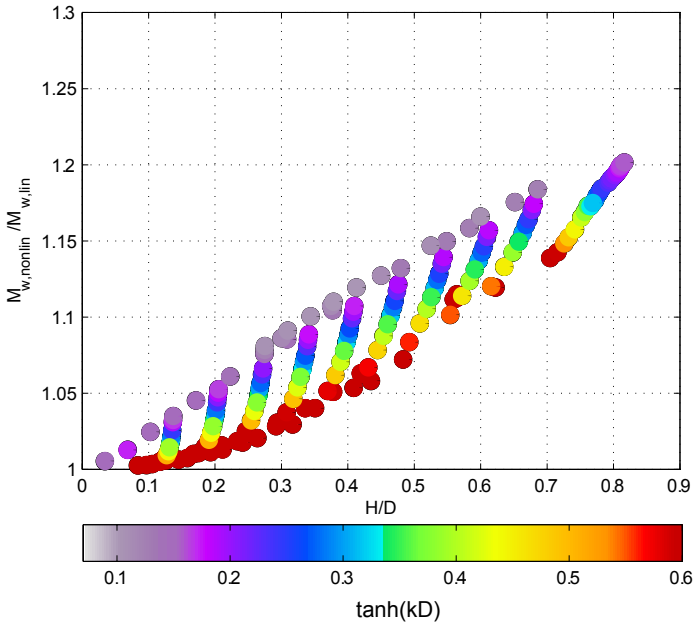

Figure 21.2: Ratio of the wave momentum for periodic waves of finite amplitude and linear waves with the same surface elevation variance. This was computed using the streamfunction theory of Dean and Dalrymple (1974) with orders 80 to 120.

These quantities are used in other relations

$$M^w = \rho_w CD - Q, \tag{21.28}$$
$$2E_c = CM^w - \rho_w \mathcal{C}, \tag{21.29}$$
$$S_{xx} = 4E_c - 3E_p + \rho_w \overline{u_b^2} + \rho_w C^2 \tag{21.30}$$
$$F = C\left(3E_c - 2E_p\right) + \frac{1}{2}\overline{u_b^2}\left(M^w + \rho_w CD\right) + C\mathcal{C}Q \tag{21.31}$$
$$K = 2\frac{\mathcal{M}}{\rho_w} + \overline{u_b^2} + C^2, \tag{21.32}$$
$$R = \frac{1}{2}K + h, \tag{21.33}$$
$$S = S_{xx} - 2CM^w + D\left(C^2 + \frac{1}{2}D\right), \tag{21.34}$$

where K is Bernoulli's constant, linked to the surface dynamic boundary condition of constant pressure along the sea surface,

$$K = (u - C) + w^2 + 2\zeta \quad \text{pour} \quad z = \zeta \tag{21.35}$$

21.2.5 Nonlinear corrections to Airy waves

Using periodic numerical solutions, one may propose empirical corrections for various quantities. For example, figure 21.2 shows the expected correction for the wave momentum M_w, as a function of the parameters H/D and kD.

21.3 Nonlinear theory for random waves

Nonlinearity of random waves has a few distinct effects on the wave spectrum. First of all, the exchange of energy between different spectral components is given by the Hasselmann (1960) theory, as introduced in chapter 8.

21.3.1 Dispersion relation

Another effect is a change in the dispersion relation. That is particularly important when measuring currents using the dispersion relation, with a HF radar, or sequences or radar or optical images. Barrick and Weber (1977) showed that for the wavenumber k_B and wave direction θ_B, a first correction of the deep water wave dispersion is (Broche et al., 1983; Ardhuin et al., 2008),

$$C_2(k_B,\theta_B) = \frac{\sqrt{g}}{2} k_B^{3/2} \int_0^\infty \int_0^{2\pi} F(x,\alpha) E(f,\theta) \mathrm{d}\theta \mathrm{d}f,$$

where, using $y = x^{1/2} = f/f_B$ and $a = \cos\alpha$,

$$F(x,\alpha) = y\left\{2a - y + 3xa\right\} + y \sum_{\varepsilon=\pm 1} \frac{\varepsilon - a}{a_\varepsilon - (1+\varepsilon y)^2} \left\{ (ya - x) \frac{a_\varepsilon + (1+\varepsilon y)^2}{2} + (1+\varepsilon y)\left(1 + \varepsilon x a + \varepsilon y\left(x + \varepsilon a\right) - a_\varepsilon\right) \right\}, \tag{21.36}$$

where

$$a_\varepsilon = \left(1 + x^2 + 2\varepsilon x a\right)^{1/2}. \tag{21.37}$$

For $x < 1$, $F(x,0) = 4x^{3/2}$, and for $x > 1$, $F(x,0) = 4x^{1/2}$ (Longuet-Higgins and Phillips, 1962). In general $F(x,\alpha) \simeq F(x,0)\cos\alpha$, with approximation errors under 5 %.

21.3.2 Harmonics

The presence of harmonics for random waves is a generalization of the harmonics for periodic waves. A first approximation, at second order, gives the harmonic corrections as a sum of interactions of the first order waves. However, to be complete in terms of spectrum, one needs to include not only the $\Phi_2^2(\mathbf{k})$ terms that are the products of linear waves $\Phi_1^2(\mathbf{k}')\Phi_1^2(\mathbf{k}-\mathbf{k}')$, but also the interactions of third order with first order $\Phi_{3,1}(\mathbf{k})\Phi_1(\mathbf{k})$ avec $\Phi_3(\mathbf{k})$. These were typically not included by Weber and Barrick (1977).

This omission is corrected in Creamer et al. (1989) and Janssen (2009). That latter approach is well suited for numerical wave modelling: the wave amplitude variables are transformed following Krasitskii (1994) to remove resonances at second order: one can then compute the evolution of the transformed wave field and then the evolved field can be transformed back to "natural variables", which is a bit like adding the second order spectrum. This approach has been particularly used to compute forces excerted by waves on structures (Prevosto and Forristall, 2002).

21.4 Non-linear 4-wave interactions

21.4.1 Deep water evolution

For a continuous wave spectrum, we find resonances that look like the forced oscillator solution in the case of the wind-generation. For evolution times much longer than the wave period, the sixth order energy term that comes from third order amplitudes

$$E_{3,3}(\mathbf{k}) = \frac{|\mathrm{d}Z_3(\mathbf{k})|^2 + |\mathrm{d}\Phi_3(\mathbf{k})|^2}{2\mathrm{d}\mathbf{k}} \tag{21.38}$$

gives an evolution equation similar to the grown of waves in the presence of wind, except that this is here for the 6th order spectrum

$$\frac{\partial E_{3,3}(\mathbf{k})\,(\mathbf{k})}{\partial t} = \frac{\pi}{2} \int |B|^2 E(\mathbf{k}_1) E(\mathbf{k}_2) E(\mathbf{k}_3) \mathrm{d}\mathbf{k}_1 \mathrm{d}\mathbf{k}_2 \mathrm{d}\mathbf{k}_3. \tag{21.39}$$

We can thus obtain the rate of change of the spectrum,

$$E(\mathbf{k}) = E_2(\mathbf{k}) + E_4(\mathbf{k}) + E_6(\mathbf{k}) + ... \tag{21.40}$$

where we have left out the odd order terms (third order, fifth order) that are exactly zero in the case of a Gaussian sea state (Hasselmann, 1962). We already know the second order terms,

$$E_2(\mathbf{k}) = 2\frac{|\mathrm{d}Z_1(\mathbf{k},+)|^2}{\mathrm{d}\mathbf{k}} \tag{21.41}$$

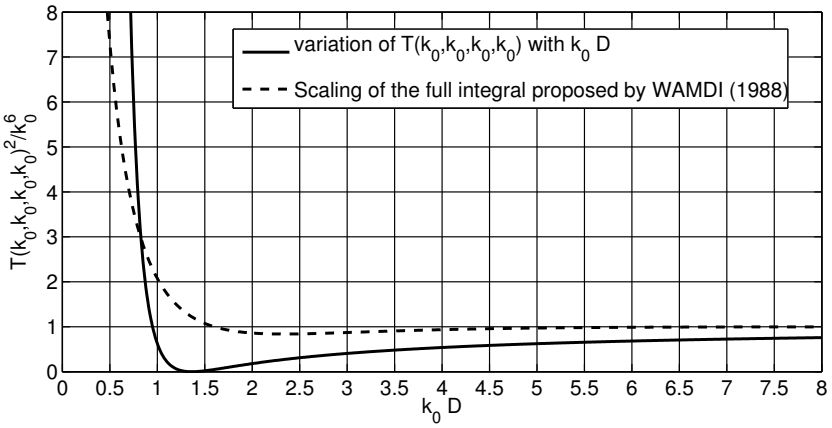

Figure 21.3: Change of the 4-wave coupling coefficient T for equal wavenumbers $k_1 = k_2 = k_3 = k_4$ as a function of the non-dimensional depth kD. The dashed line is the parameterization proposed by the WAMDI Group(1988), and the solid line is the result by Janssen and Onorato (2007).

and at 4th order the energy is not equally split between potential and kinetic energy so we have to add these two separately,

$$E_4(\mathbf{k}) = \frac{1}{2\mathrm{d}\mathbf{k}} \left\{ \overline{|\mathrm{d}Z_2(\mathbf{k})|^2} + 2\mathcal{R}\left[\overline{Z_1(-\mathbf{k})Z_3(\mathbf{k})}\right] + \frac{\sigma^2}{g^2}\overline{|\mathrm{d}\Phi_2(\mathbf{k})|^2} + 2\frac{\sigma^2}{g^2}\mathcal{R}\left[\overline{\Phi_1(-\mathbf{k})\Phi_3(\mathbf{k})}\right] \right\} \tag{21.42}$$

and we now have the 6th order term that have a long-term evolution,

$$\begin{aligned} E_6(\mathbf{k}) \quad = \quad & \frac{1}{2\mathrm{d}\mathbf{k}} \left\{ \overline{|\mathrm{d}Z_3(\mathbf{k})|^2} + 2\mathcal{R}\left[\overline{Z_1(-\mathbf{k})Z_5(\mathbf{k})}\right] + 2\mathcal{R}\left[\overline{Z_2(-\mathbf{k})Z_4(\mathbf{k})}\right] \right. \\ & \left. + \frac{\sigma^2}{g^2}\overline{|\mathrm{d}\Phi_3(\mathbf{k})|^2} + 2\frac{\sigma^2}{g^2}\mathcal{R}\left[\overline{\Phi_1(-\mathbf{k})\Phi_5(\mathbf{k})}\right] + 2\frac{\sigma^2}{g^2}\mathcal{R}\left[\overline{\Phi_2(-\mathbf{k})\Phi_4(\mathbf{k})}\right] \right\} \end{aligned} \tag{21.43}$$

This means that to do this right, one has to carry out the calculations of the amplitudes to 5th order, which was first done by Hasselmann (1962).

21.4.2 4-wave interactions in shallow water

As the water depth goes down, the interactions change shape because the wave kinematics and dispersion relation change. (Janssen and Onorato, 2007) have shown that the previously proposed use of a DIA approximation with a coupling coefficient varying as a function of kD may not work so well. Indeed the coupling coefficient T for $k_1 = k_2 = k_3 = k_4$ goes to zero at the depth $kD = 1.363$, and is much weaker than in deep water when $1.2 < kD < 3$, as shown in Fig. 21.3). There is still much debate on how to properly represent finite depth effects on 4-wave interactions.

Chapter 22

Waves at second order

22.1 Equations of motion at second order

From the full Bernoulli equation (21.1), the second order approximation is

$$\frac{\partial \phi_2}{\partial t} = -\frac{1}{2}\left[|\boldsymbol{\nabla}\phi_1|^2 + \left(\frac{\partial \phi_1}{\partial z}\right)^2\right] - \frac{p_2}{\rho_w} - gz + C_2(t). \tag{22.1}$$

The usual combination with the surface kinematic boundary condition yields the second order wave equation,

$$\left(\frac{\partial^2}{\partial t^2} + \frac{\partial}{\partial z}\right)\phi_2 + g\frac{\partial \phi_2}{\partial z} = -g\zeta_1\frac{\partial^2 \phi_1}{\partial z^2} + g\boldsymbol{\nabla}\phi_1 \cdot \boldsymbol{\nabla}\zeta_1 - \frac{\partial}{\partial t}\left(\zeta_1\frac{\partial^2 \phi_1}{\partial z \partial t}\right) - \boldsymbol{\nabla}\phi_1 \cdot \frac{\partial \boldsymbol{\nabla}\phi_1}{\partial t} - \frac{\partial \phi_1}{\partial z}\frac{\partial^2 \phi_1}{\partial t \partial z} \quad \text{on} \quad z = 0.$$

The first term on the right hand side comes from the Taylor expansion of the left hand side around $z = 0$, and the four other terms are coming from eq. (21.3).

22.2 Monochromatic waves at second order

Plugging a single monochromatic wave solution with wavenumber $\mathbf{k}_0$, as given in chapter 2, gives second order Stokes solution. For a linear amplitude $a = 2Z^+_{1,\mathbf{k}_0}$, we have $\Phi^+_{1,\mathbf{k}_0} = -\mathrm{i}ag/(2\sigma)$ and

$$\phi_1 = \frac{\cosh(k_0 z + k_0 h)}{\cosh(k_0 D)}\left(\Phi^+_{1,\mathbf{k}_0}\mathrm{e}^{\mathrm{i}(\mathbf{k}_0\cdot\mathbf{x} - \sigma_0 t)} + \overline{\Phi}^+_{1,\mathbf{k}_0}\mathrm{e}^{-\mathrm{i}(\mathbf{k}_0\cdot\mathbf{x} - \sigma_0 t)}\right), \tag{22.2}$$

The solution is,

$$\phi_2 = \frac{\cosh(2k_0 z + 2k_0 h)}{\cosh(2k_0 D)}\left(\Phi^+_{2,2\mathbf{k}_0}\mathrm{e}^{\mathrm{i}(2\mathbf{k}_0\cdot\mathbf{x} - 2\sigma_0 t)} + \overline{\Phi}^+_{2,2\mathbf{k}_0}\mathrm{e}^{-\mathrm{i}(2\mathbf{k}_0\cdot\mathbf{x} - 2\sigma_0 t)}\right) + 2\Phi^+_{2,\mathbf{0}} \tag{22.3}$$

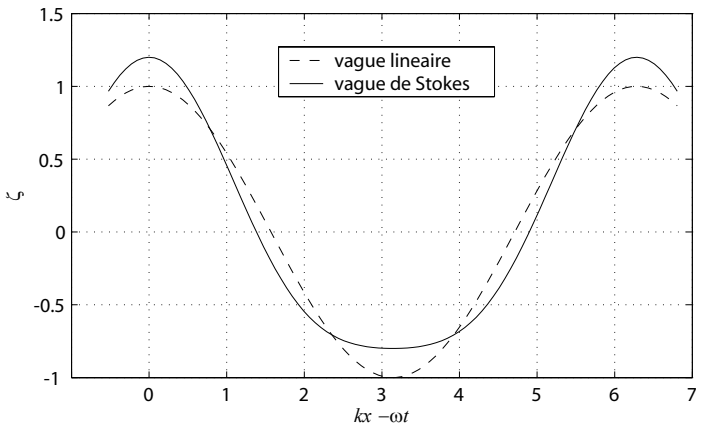

Figure 22.1: Profiles of a linear Airy wave and a second order Stokes wave.

avec

$$\Phi^+_{2,2\mathbf{k}_0} = D(\mathbf{k}_0,\mathbf{k}_0)\frac{\left(\Phi^+_{1,\mathbf{k}_0}\right)^2}{\sigma^2(2k_0)-4\sigma_0^2} \tag{22.4}$$

$$= \frac{3\mathrm{i}\sigma k\cosh(2kD)}{4g\sinh^3(kD)\cosh(kD)}\left(\Phi^+_{1,\mathbf{k}_0}\right)^2, \tag{22.5}$$

and

$$\Phi^+_{2,\mathbf{0}} = 0, \tag{22.6}$$

giving

$$Z^+_{2,2\mathbf{k}_0} = a^2\frac{k\cosh(kD)\left[2+\cosh(2kD)\right]}{32\sinh^3(kD)}, \tag{22.7}$$

and

$$Z^+_{2,\mathbf{0}} = a^2\frac{\sigma^2}{g^2}k^2\left[\tanh^2(2kD)-1\right]. \tag{22.8}$$

The phases of the harmonics are locked with the phase of the linear waves, and the elevation and velocity fields are given by (Dean and Dalrymple, 1991),

$$\zeta = a\cos\left[k(x-Ct)\right] + ka^2\frac{\left[2+\cosh(kD)\right]}{4\sinh^3(kD)}\cos\left[2k(x-Ct)\right] \tag{22.9}$$

$$u = \omega a\frac{\cosh(kz+kD)}{\sinh(kD)}\cos\left[k(x-Ct)\right] + \frac{3}{4}k^2a^2C\frac{\cosh(2kz+2kD)}{\sinh^4(kD)}\cos\left[2k(x-Ct)\right] \tag{22.10}$$

Compared to linear waves, this orbital velocity is higher at the crests, and lower under the troughs.

22.3 Second order motion for random waves

Before generalizing to a full wave spectrum, we note tha Miche (1944) provided the solution for two monochromatic wave trains in opposite directions, which gives a non-zero contribution $C_2(t)$. The general second-order solution, first given by Biesel (1952), comes from using a full superposition of linear waves for ϕ_1 and ζ_1, which are related by the linear polarization relation given in chapter 2. Here we generally follow the notations used by Hasselmann (1962).

The dynamic and kinematic boundary conditions a the free surface $z=\zeta$ are

$$p = p_a \tag{22.11}$$

$$w = \frac{\partial\phi}{\partial z} = \boldsymbol{\nabla}\phi\cdot\boldsymbol{\nabla}\zeta + \frac{\partial\zeta}{\partial t}. \tag{22.12}$$

As done in chapter 2, we move the boundary condition on $z=\zeta$ to an equation on $z=0$ with a Taylor expansion

$$\frac{\partial\zeta}{\partial t} - \frac{\partial\phi}{\partial z} \simeq \boldsymbol{\nabla}\phi\cdot\boldsymbol{\nabla}\zeta + \zeta\frac{\partial^2\phi}{\partial^2 z} \quad \text{on} \quad z=0. \tag{22.13}$$

Again the combination of eq. (23.10) at $z=\zeta$, where $p=p_a$, and (22.13) allows us to remove the unknown ζ,

$$\left[\left(\frac{\partial^2}{\partial t^2}+g\frac{\partial}{\partial z}\right)\phi_2\right]_{z=0} = -\frac{\partial}{\partial t}\left(\frac{p_a}{\rho_w}\right) - \frac{1}{2}\left\{\frac{\partial}{\partial t}\left[|\boldsymbol{\nabla}\phi|^2 + \left(\frac{\partial\phi}{\partial z}\right)^2 + 2\zeta\frac{\partial^2\phi}{\partial t\partial z}\right]\right\}_{z=0} - g\left\{\boldsymbol{\nabla}\phi\cdot\boldsymbol{\nabla}\zeta + \zeta\frac{\partial^2\phi}{\partial^2 z}\right\}_{z=0}. \tag{22.14}$$

We now replace by the forcing by the first order solution to obtain the forced second order wave equation

$$\left[\left(\frac{\partial^2}{\partial t^2}+g\frac{\partial}{\partial z}\right)\phi_2\right]_{z=0} = \frac{\partial}{\partial t}\left\{-\frac{p_a}{\rho_w} - \sum_{\mathbf{k},s}\sum_{\mathbf{k}',s'}\frac{D(\mathbf{k},\mathbf{k}')}{\mathrm{i}(s\sigma+s'\sigma')}\Phi^s_{1,\mathbf{k}}\Phi^{s'}_{1,\mathbf{k}'}\mathrm{e}^{\mathrm{i}\left[(\mathbf{k}+\mathbf{k}')\cdot\mathbf{x}-(s\sigma+s'\sigma')t\right]}\right\}, \tag{22.15}$$

where the coupling coefficient $D(\mathbf{k},\mathbf{k}')$ is given by Hasselmann (1962),

$$D(\mathbf{k},\mathbf{k}') = \mathrm{i}(s\sigma+s'\sigma')\left[kk'\tanh(kD)\tanh(k'h)-\mathbf{k}\cdot\mathbf{k}'\right] - \frac{\mathrm{i}}{2}\left(s\sigma\frac{k'^2}{\cosh^2(k'h)} + s'\sigma'\frac{k^2}{\cosh^2(kD)}\right). \tag{22.16}$$

As noted by Hasselmann (1963), the forcing terms in the equations are equivalent to a pressure term $\widehat{p}_2$. Replacing $\Phi^s_{1,\mathbf{k}}$ by $-\mathrm{i}sgZ^s_{1,\mathbf{k}}/\sigma$ it is

$$\begin{aligned}\widehat{p}_2 &= -\rho_w \sum_{\mathbf{k},s,\mathbf{k}',s'} \left\{ s\sigma s'\sigma' \left[1 - \frac{\mathbf{k}\cdot\mathbf{k}'}{kk' \tanh(kD)\tanh(k'h)} \right] \right. \\ &\left. - \frac{1}{2(s\sigma + s'\sigma')} \left(\frac{g^2 k'^2}{s'\sigma' \cosh^2(k'h)} + \frac{g^2 k^2}{s\sigma \cosh^2(kD)} \right) \right\} Z^s_{1,\mathbf{k}} Z^{s'}_{1,\mathbf{k}'} \mathrm{e}^{\mathrm{i}\left[(\mathbf{k}+\mathbf{k}')\cdot\mathbf{x} - (s\sigma + s'\sigma')t\right]} \end{aligned} \tag{22.17}$$

The nice symmetric form of $D(\mathbf{k}_1, \mathbf{k}_2)$ given by eq. (22.16) can be obtained as follows. One can first expand the products such as $\boldsymbol{\nabla}\phi_1 \cdot \boldsymbol{\nabla}\zeta_1$,

$$\boldsymbol{\nabla}\phi_1 \cdot \boldsymbol{\nabla}\zeta_1|_{z=0} = \sum_{\mathbf{k}_1, s_1} \mathrm{i}\mathbf{k}_1 \Phi^{s_1}_{1,\mathbf{k}_1} \mathrm{e}^{\mathrm{i}(\mathbf{k}_1\cdot\mathbf{x} - s_1\sigma_1 t)} \cdot \sum_{\mathbf{k}_2, s_2} \mathrm{i}\mathbf{k}_2 Z^{s_2}_{1,\mathbf{k}_2} \mathrm{e}^{\mathrm{i}(\mathbf{k}_2\cdot\mathbf{x} - s_2\sigma_2 t)}, \tag{22.18}$$

then replacing $Z^{s_2}_{1,\mathbf{k}_2}$ by $\mathrm{i}s_2\sigma_2\Phi^{s_2}_{1,\mathbf{k}_2}/g$, and collecting the terms

$$\boldsymbol{\nabla}\phi_1 \cdot \boldsymbol{\nabla}\zeta_1|_{z=0} = \sum_{\mathbf{k}_1, \mathbf{k}_2, s_1, s_2} -\mathrm{i}\mathbf{k}_1\cdot\mathbf{k}_2 \frac{s_2\sigma_2}{g} \Phi^{s_1}_{1,\mathbf{k}_1} \Phi^{s_2}_{1,\mathbf{k}_2} \mathrm{e}^{\mathrm{i}\left[(\mathbf{k}_1+\mathbf{k}_2)\cdot\mathbf{x} - (s_1\sigma_1 + s_2\sigma_2)t\right]}. \tag{22.19}$$

To get the symmetry, the trick is to write the two sums with $\mathbf{k}_1$ and $\mathbf{k}_2$ switched or not, and take half of their sum,

$$\boldsymbol{\nabla}\phi_1 \cdot \boldsymbol{\nabla}\zeta_1|_{z=0} = \sum_{\mathbf{k}_1, \mathbf{k}_2, s_1, s_2} -\mathrm{i}\mathbf{k}_1\cdot\mathbf{k}_2 \frac{s_1\sigma_1 + s_2\sigma_2}{2g} \Phi^{s_1}_{1,\mathbf{k}_1} \Phi^{s_2}_{2,\mathbf{k}_2} \mathrm{e}^{\mathrm{i}\left[(\mathbf{k}_1+\mathbf{k}_2)\cdot\mathbf{x} - (s_1\sigma_1 + s_2\sigma_2)t\right]}. \tag{22.20}$$

22.4 Pressure at second order

Using the coupling coefficient D given by Hasselmann (1962, eq. 4.3) for the velocity potentials, our coupling coefficient for the elevation amplitudes is

$$\begin{aligned} D_z(\mathbf{k}, s, \mathbf{k}', s') &= -\frac{g^2 D(\mathbf{k}, s, \mathbf{k}', s')}{\mathrm{i}s\sigma s'\sigma'(s\sigma + s'\sigma')} \\ &= \frac{g^2}{s\sigma s'\sigma'} \left\{ \left[\mathbf{k}\cdot\mathbf{k}' - \frac{\sigma^2\sigma'^2}{g^2} \right] + \frac{0.5}{(s\sigma + s'\sigma')} \left(\frac{s\sigma k'^2}{\cosh^2(k'h)} + \frac{s'\sigma' k^2}{\cosh^2(kD)} \right) \right\} \end{aligned} \tag{22.21}$$

In the bottom pressure, the additional term arising from the orbital velocity has a coupling coefficient

$$D_{pb}(\mathbf{k}, s, \mathbf{k}', s', z) = g^2 \frac{kk' \sinh[k(z+h)] \sinh[k'(z+h)] - \mathbf{k}\cdot\mathbf{k}' \cosh[k(z+h)] \cosh[k'(z+h)]}{2s\sigma s'\sigma' \cosh(kD) \cosh(k'h)}. \tag{22.22}$$

The relationship with the coupling coefficient C given by Herbers and Guza (1991, their eq. 4) for the bottom pressure, is given by solving eq. (22.15) for ϕ_2, and then rewriting Bernoulli's equation (23.10), as

$$\frac{p_2}{\rho_w} = \frac{\partial\phi_2}{\partial t} - \frac{1}{2}\left[|\boldsymbol{\nabla}\phi_1|^2 + \left(\frac{\partial\phi_1}{\partial z} \right)^2 \right] \tag{22.23}$$

This gives, for $z = -h$,

$$C = -\frac{D_z(s\sigma + s'\sigma')^2}{g\left[gK\tanh(KD) - (s\sigma + s'\sigma')^2\right]} + \frac{D_{pb}(z=-h)}{g}. \tag{22.24}$$

ϕ_2 is a solution to Laplace equation and the bottom boundary condition, and its Fourier component $\Phi_{2,\mathbf{k}}$ for the wavenumber $\mathbf{k}$ thus has a vertical structure that is the same as that of ϕ_1, namely it is proportional to $\cosh(kz + kD)$. The Fourier transform of eq. (22.15) thus gives for each $\mathbf{k}$

$$\frac{\partial^2\Phi_{2,\mathbf{k}}}{\partial t^2} + gk\tanh(kD)\,\Phi_{2,\mathbf{k}} = \sum_{\mathbf{k}_1+\mathbf{k}_2=\mathbf{k}, s_1, s_2} D(\mathbf{k}_1, \mathbf{k}_2)\,\Phi^{s_1}_{1,\mathbf{k}_1} \Phi^{s_2}_{1,\mathbf{k}_2} \mathrm{e}^{\mathrm{i}-(s_1\sigma_1 + s_2\sigma_2)t}. \tag{22.25}$$

The amplitudes $Z_{2,\mathbf{k}}$ of the second order surface elevation ζ_2 are given by the surface kinematic boundary condition at second order,

$$Z_{2,\mathbf{k}} = -\frac{1}{g}\frac{\partial \Phi_{2,\mathbf{k}}}{\partial t} + \sum_{\mathbf{k}_1+\mathbf{k}_2=\mathbf{k},s_1,s_2} G\left(\mathbf{k}_1,\mathbf{k}_2\right)\Phi^{s_1}_{1,\mathbf{k}_1}\Phi^{s_2}_{1,\mathbf{k}_2}\mathrm{e}^{-\mathrm{i}(s_1\sigma_1+s_1\sigma_1)t}. \tag{22.26}$$

with the coupling coefficient G given by Hasselmann (1962),

$$G\left(\mathbf{k}_1,\mathbf{k}_2\right) = \frac{1}{2g}\left[\mathbf{k}_1\cdot\mathbf{k}_2 - g^{-2}s_1s_2\sigma_1\sigma 2\left(\sigma_1^2+\sigma_2^2+s_1s_2\sigma_1\sigma_2\right)\right]. \tag{22.27}$$

The forced oscillation equation (22.25) has no resonant forcing term because the dispersion relation gives $\sigma\left(\mathbf{k}_1+\mathbf{k}_2\right) \neq \sigma\left(\mathbf{k}_1\right)+\sigma\left(\mathbf{k}_2\right)$ except in the limit of shallow water $kD \to 0$, or in the case of gravity-capillary waves. Except for these two cases, the second order waves have bound amplitudes given as a double-sum of first order - first order interactions. This bound second order solution can lead to oscillations of the amplitudes in time, known as "recurrences" (Fermi et al., 1955).

22.5 The second order spectrum

Because the wave spectrum is a quadratic quantity, the expansion of the surface elevation up to third order

$$\zeta = \zeta_1 + \zeta_2 + \zeta_3 + ... \tag{22.28}$$

is needed to evaluate what is often called the second order spectrum, but that is in fact a fourth order quantity. The fourth order elevation variance is

$$E = \overline{\zeta_1+\zeta_2+\zeta_3+...}^2 = \overline{\zeta_1^2} + 2\overline{\zeta_1\zeta_2} + \overline{\zeta_2^2} + 2\overline{\zeta_1\zeta_3} + ... \tag{22.29}$$

Chapter 23

Ocean waves and microseisms

An updated and more complete version of this chapter can be found in Ardhuin et al. (2019). The generation and propagation of microbaroms, which are atmospheric acoustic waves, will be treated in a chapter 24.

23.1 A short history of microseism observations

In the early days of seismology in the late 19th century, a background noise of varying amplitude was detected. Bertelli (1872) performed measurements in Italy and found that the amplitude of these microseisms changed with the passing of storms. By the year 1900, the phenomenon was measured all around the globe, and Algué (1900) related measurements in the Philippines to the passage of Typhoons. Many observations followed and the investigation of microseisms has grown to been a big branch of seismology. What was a curiosity is now an important source of data for studying the Earth's structure as microseisms provide a continuous source of signals that can be used to infer properties of the solid Earth (Shapiro et al., 2005) or to investigate the ocean wave climate (Zopf et al., 1976) because, yes, microseisms are generated by ocean waves, we will see how this happens.

All seismometer measurements on Earth contain microseisms. These seismic waves propagate through the solid Earth and oceans, with a displacement amplitude that rarely exceeds 10 microns, and a dominant wave period typically between 3 and 10 s.

From seismograph records, the apparently random signal gives a power spectrum with very robust features. Stutzmann et al. (2000) showed how the noise level generally decreases from island stations to stations deep inside continents, with a classical shape. When the vertical acceleration is considered, the noise generally has 2 broad peaks. The so-called 'secondary' peak lies at periods between 3 and 10 s, typically half of the dominant ocean wave periods, and it is the most energetic. The weaker 'primary' peak has the same period as typical swells, between 10 and 25 s, and a broad interval of noise is found at periods above 30 s. That long period range is called the hum.

In all of these frequency bands, the seismic waves can be separated in different modes,

- Raleigh waves: these are waves that follow the surface of the crust, with a motion in the plane of propagation, and an exponential decrease of the motion amplitude towards the center of the Earth. Within 2000 km from the source, these Rayleigh waves usually dominate the microseisms recorded in the 3 to 10 s period band.
- Love waves: these are waves that follow the surface of the crust, with a motion out of the plane of propagation, and an exponential decrease of the motion amplitude towards the center of the Earth.
- compressive body (P) waves: these waves travel through the Earth mantle, with a motion in the direction of propagation.
- shear body (S) waves: these waves travel through the Earth mantle, with a motion transverse to the direction of propagation, either in the vertical direction, these are then called SV waves, or horizontal direction, and they are called SH waves.

Ongoing efforts are now explaining how and where this noise comes from, which may have some important application for seismology or the study of the ocean wave climate. The acoustic noise field in

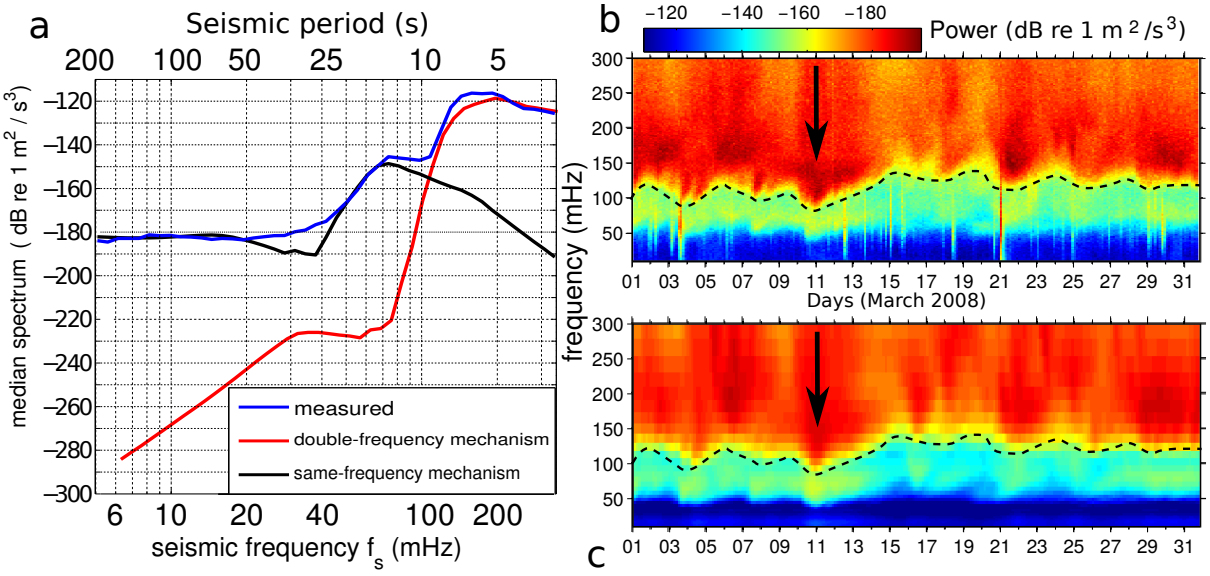

Figure 23.1: Measured and modeled seismic spectra. (a) Median vertical acceleration power spectra in March 2008 at the French SSB seismic station, located near Saint-Etienne, France. (b) observed and (c) modeled spectra in March 2008 following Ardhuin et al. (2015). Light blue to red vertical stripes correspond to earthquakes (not modeled). Contrary to intuition, the direct impact of waves at the shoreline shown on these pictures is not the main source of the microseisms recorded at remote stations. Instead, seismic waves are mostly generated by two mechanisms: a same-frequency mechanism involves wave propagation over varying topography in intermediate water depth, and a double-frequency mechanism that involves the interaction of waves in opposite directions. The dashed line separates the low frequencies where the same-frequency mechanism dominates from the higher frequencies explained by the double-frequency mechanism. The Johanna storm, marked by the vertical arrow on March 10, is conspicuous with powerful and low frequency microseisms.

the ocean is also part of this seismic noise field, with some wave modes that have important signatures in the water column and in the atmosphere.

A key feature of the generation of microseisms is that it transfers energy from ocean waves that are slow, with typical phase speeds of 10 m/s, to the much faster seismic waves with speeds of several km/s. How can slow waves excite fast waves?

23.2 The particular case of standing ocean waves

Miche (1944) was the first to show that, at second order in the wave steepness, the pressure under stationary waves oscillates in time but does not decay with depth. Clearly, we cannot generally assume that $C(t)$ in the Bernoulli equation is zero. Taking two propagating waves that give standing waves, with elevations $a\cos(kx-\sigma t)$ and $a\cos(kx+\sigma t)$, going in directions towards $x>0$ and $x<0$. Their sum is the stationary wave,

$$\zeta = 2a\cos(kx)\cos(\sigma t). \tag{23.1}$$

$$w = -2a\sigma\frac{\sinh(kz+kD)}{\sinh(kD)}\cos(kx)\sin(\sigma t). \tag{23.2}$$

$$\tag{23.3}$$

It is particulary interesting to look at the horizontally averaged pressure at depth z using eq. (10.30)

$$\overline{p}(z) = \rho_w g(\zeta - z) + \rho_w \frac{\partial}{\partial t}\overline{\zeta w(\zeta)} - \rho_w \overline{w(z)^2}. \tag{23.4}$$

The last two terms are deviations from the hydrostatic pressure and they give the non-hydrostatic (NH) pressure,

$$\overline{p}_{\rm NH}(z) = -2\rho_w a^2\sigma^2\left[\cos(2\sigma t) + \frac{\sinh^2(kz+kD)}{\sinh^2(kD)}\sin^2(\sigma t)\right]. \tag{23.5}$$

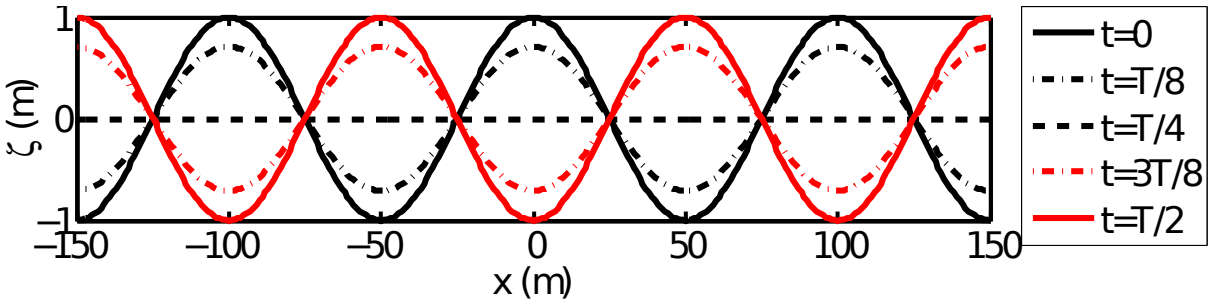

Figure 23.2: Schematic positions of the free surface in a stationary wave at different phases of the period T of the progressive wave.

While the second term does not oscillate in time and decays with depth, the first term oscillates at a period equal to half of the propagating wave period, but is uniform over the vertical.

This fluctating pressure, predicted by Miche (1944), was interpreted by Longuet-Higgins (1950) as the vertical force that is necessary to compensate the fluctuations of the vertical momentum per unit surface

$$M_z = \overline{\int_{-h}^{\zeta} \rho_w w \mathrm{d}z} \simeq \rho_w \overline{\zeta w(\zeta)}. \tag{23.6}$$

This momentum is only non-zero when w and ζ are correlated, and at depth $dM_z/dt = p_{\mathrm{NH}}(z \to \infty)$.

It should be noted, also, that the first term in pressure $\overline{p}_{\mathrm{NH}}$ is lowest when the wave amplitude is maximum, contrary to the second term. In the limit of shallow water $kD \ll 1$ and we have $\overline{p}_{\mathrm{NH}}(z) = 0$.

Of course, the surface pressure is not immediately transmitted at large depth, and a more detailed description requires to take into account the compressibility of sea water. In reality, the surface oscillations produce acoustic waves that radiate in the water column (Longuet-Higgins, 1950), and are easily recorded at the ocean bottom (Farrell and Munk, 2008). Eq. (23.5) was verified in the laboratory by Cooper and Longuet-Higgins (1951).

Compared to the classical studies of ocean waves, the investigation of seismic and acoustic noise requires to relax two of the hypothesis made in chapter 2. Namely, we will have to take into accound the compressibility of sea water and air, and we will also need to allow the sea bottom to deform under the varying water pressure.

In the case of exactly standing waves, the associated acoustic waves is propagating along the vertical. So this is not yet giving the seismic Rayleigh waves observed on land as surface waves. But the ocean waves are not monochromatic, so that it is much more likely to have interactions of waves with different wavenumbers rather than waves with exactly opposing direction and frequency. In fact, mathematically, the weight of these exactly opposing waves is zero. We thus need to generalize the standing wave to what we will find to be supersonic wave groups in the next section.

23.3 Wave-wave interaction theory for microseism generation

Here we generally follow the method of Hasselmann (1963) with several corrections exposed by Ardhuin and Herbers (2013). In this process we also compute properties of Rayleigh waves in the presence of a water layer, which was first done by Stoneley (1926), and is covered in seismology textbooks such as Lay and Wallace (1995),page 133, note the typo with ρ_w and ρ_s exchanged in the dispersion relation.

23.3.1 Wavenumber diagrams and isotropy of microseism sources

We have seen in the previous chapters that wave components of frequency f and wavenumber vector $\mathbf{k}$ can interact with another wave or a change in medium (water depth or current) that has a frequency f' and wavenumber $\mathbf{k}'$, giving rise to a wave of frequency $f_s = f + f'$ and wavenumber $\mathbf{K} = \mathbf{k} + \mathbf{k}'$. The general theory of such interactions was sumarized by Hasselmann (1966).

If the phase speed $2\pi(f + f')/|\mathbf{k} + \mathbf{k}'|$ matches the speed of a seismic mode, then there is a resonance and interaction of waves with that seismic mode. In the case of microseisms, the ocean waves transfer energy to the seismic wave. Conversely, the vertical shaking of water, usually in the laboratory, gives rise to standing waves in the water, also known as Faraday waves.

For seismic frequencies f_s around 0.2 Hz, the phase speed of seismic waves is larger 1.5 km/s, such large speed can only be achieved if $K << k$, which imposes $\mathbf{k}' \simeq -\mathbf{k}$, as illustrated on figure 23.3. The two neear-resonant configurations produce seismic waves that travel in very different directions. However, compared to that of the ocean waves, a 1% change in the wave vector $\mathbf{k}$ is generally negligible, because the half-width of the wave spectrum in frequency and direction is generally of the order of 5% or more, and the wave energy spectral density $E(f, \theta)$ is the same if $\mathbf{k}$ changes by only 1%. Hence, at the spectral peak, the source of microseisms is isotropic.

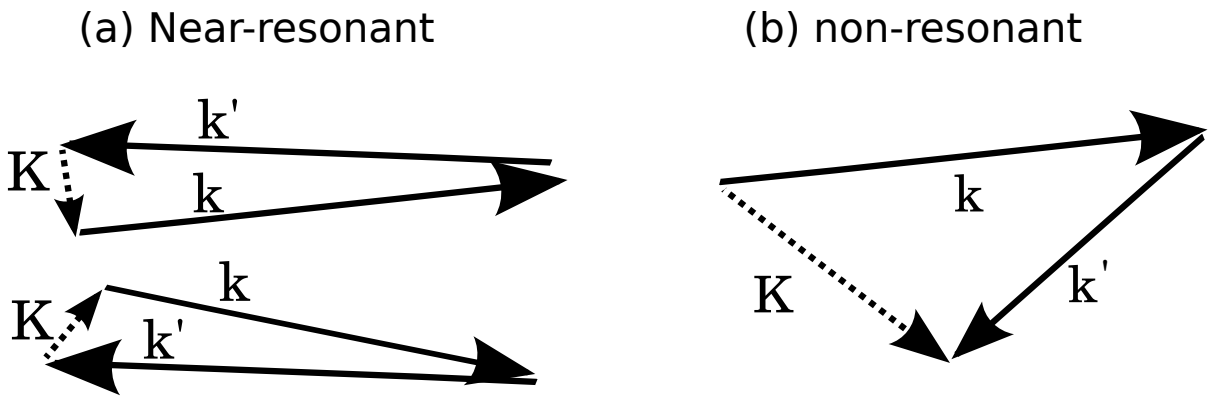

Figure 23.3: Typical configuration of interacting wave components

We can distinghish two mechanisms that give rise to these interactions,

- A same-frequency mechanism: $\mathbf{k}'$ corresponds to a change in depth or current, this is usually fixed in time or at least much slower than the waves, hence $f' = 0$ and $f_s = f$, the seismic waves have the same frequency as the ocean waves.
- A double-frequency mechanism: $\mathbf{k}'$ corresponds to another wave component. Since $\mathbf{k}' \simeq -\mathbf{k}$, we also have $|\mathbf{k}'| \simeq |\mathbf{k}|$ and $f \simeq f'$, thus $f_s \simeq 2f$: the microseism have a frequency that is the double of the ocean wave frequency.

Figure 23.1 shows that the same-frequency mechanism only explains the hum and primary microseism, while the double-frequency mechanism explains the higher frequency secondary peak. We will now give more theoretical details for each mechanism.

23.3.2 Motion in the water and equivalent wave-induced pressure

We follow here the theory of Hasselmann (1963) made for waves in deep water ($kD >> 1$), including the correction by Ardhuin and Herbers (2013) for finite water depth. We also note that a more detailed description is detailed for the case of the atmospheric pressure in chapter 24 about microbaroms.

From Longuet-Higgins (1950), we know that at first order the wave motion is given by Airy theory as exposed in chapter 2. At second order, the motion is forced at the surface by the interaction of pairs of linear (first order) solutions. This is thus the exact same problem that is solved in chapter 21, with the only change caused by compressibility.

We decompose the water density into a mean value ρ_w and a perturbation $\rho \ll \rho_w$. Neglecting stratification effects due to temperature and salinity, the fluctuations in pressure p and water density ρ are related by an equation of state, which involves the speed of sound in water α_w (Lighthill, 1978, eq. 32).

$$\frac{dp}{dt} = \alpha_w^2 \frac{d\rho}{dt}, \tag{23.7}$$

We still assume that the motion is irrotational so that the velocity field is still given by the gradient of the velocity potential ϕ. The conservation of mass of sea water is

$$\frac{d\rho}{dt} = -\rho_w \nabla^2 \phi - \rho_w \frac{\partial^2 \phi}{\partial z^2}. \tag{23.8}$$

Equations (23.8)–(23.7) can be combined to eliminate ρ,

$$\frac{dp}{dt} = -\rho_w \alpha_w^2 \left[\nabla^2 + \frac{\partial^2}{\partial z^2}\right] \phi \tag{23.9}$$

From eq. (23.7), the water density is only a function of the pressure. The two unknowns p and ϕ are also related by the momentum conservation equation, with can be cast in the form of Bernoulli's equation (see e.g. Lamb, 1932, section 20),

$$\frac{\partial \phi}{\partial t} = -\frac{1}{2}\left[|\boldsymbol{\nabla}\phi|^2 + \left(\frac{\partial \phi}{\partial z}\right)^2\right] - \frac{p}{\rho_w} - gz + C(t), \tag{23.10}$$

with $C(t)$ a time-varying but spatially uniform function.

Therefore, instead of our usual Laplace equation we now have this acoustic wave equation in the body of the fluid (Brekhovskikh et al., 1973),

$$\frac{\partial^2 \phi}{\partial t^2} - \alpha_w^2 \nabla_3^2 \phi = -\frac{\partial}{\partial t}(\nabla_3 \phi)^2 - g\frac{\partial \phi}{\partial z}. \tag{23.11}$$

Where ∇_3 is the 3-component nabla operator. If you remember chapter 2, this is the equation that will give us the vertical structure of the wave field, which is now an acoustic wave field.

Now, in the case of microseisms, Longuet-Higgins (1950) has shown that the non-linear forcing terms in the acoustic wave equation (23.11) produce negligible terms when $\sigma \simeq 0.5$ s^{-1}, so that we can use the linearized acoustic wave equation for the second order velocity potential ϕ_2,

$$\left[\frac{\partial^2}{\partial t^2} + \alpha_w^2\left(\nabla^2 + \frac{\partial^2}{\partial z^2} - \frac{g}{\alpha_w^2}\frac{\partial}{\partial z}\right)\right]\phi_2 = 0 \quad for \quad -h \leq z \leq 0. \tag{23.12}$$

But if you really want to know more about the effect of these extra terms, do not worry, they cannot be neglected in the atmosphere when we consider microbaroms in chapter 24.

With these approximations, The link between the ocean waves and the acoustic waves only comes from the boundary conditions. As noted by Hasselmann (1963), in the surface boundary condition, the interaction of first order wave motion is equivalent to a surface pressure $\widehat{p}_2$ given by eq. (22.17). We note that this is not the true atmospheric pressure, for that you can go to chapter 24, but the pressure that is goes into the surface boundary condition for ϕ_2 and that makes it equivalent to a situation with a flat sea surface with $\widehat{p}_2$ imposed on the surface. We note that the last term of eq. (22.17) was absent in Hasselmann (1963) because he only considered waves in deep water where $kD \gg 1$. As a result, that is also missing in Webb (2007) and was corrected by Ardhuin and Herbers (2013). These authors also found a source of acoustic energy in the bottom boundary condition.

Using (22.17) the spectrum of the equivalent surface pressure can be expressed in terms of quadratic products of the (linear) sea surface elevation spectrum

$$E(k_x, k_y) = 2 \lim_{|d\mathbf{k}|\to 0} \frac{\left|Z^+_{1,\mathbf{k}}\right|^2}{\mathrm{d}k_x \mathrm{d}k_y} \tag{23.13}$$

with a coupling coefficient given by eq. (22.21) that simplifies for $K \simeq 0$ to

$$D_z\left(\mathbf{k}, 1, -\mathbf{k}, 1\right) = -2\sigma^2\left[1 + \frac{1}{4\sinh^2(kh)}\right]. \tag{23.14}$$

For any value of kD, the coupling coefficient given by eq. (23.14) differs from the full second order coefficient for the bottom pressure (e.g. eq. 4 in Herbers and Guza, 1991), which also involves the Bernoulli head (the bracket in eq. 23.10). However, that extra term is also relevant to the generation of seismic noise due to the bottom boundary condition that couples the solid crust to the water column. Indeed, the second-order pressure perturbation at the bottom writes,

$$p_2(-h) = -\rho_w \frac{\partial \phi_2}{\partial t} + \widehat{p}_{2,\mathrm{bot}}, \tag{23.15}$$

where the Bernoulli head contribution to the pressure can be expressed from the first order wave amplitudes,

$$\widehat{p}_{2,\mathrm{bot}} = \rho_w \sum_{\mathbf{k},s,\mathbf{k}',s'} D_{pb}\left(\mathbf{k}, s, \mathbf{k}', s', z = -h\right) Z^s_{1,\mathbf{k}} Z^{s'}_{1,\mathbf{k}'} \mathrm{e}^{\mathrm{i}\Theta(\mathbf{k},\mathbf{k}',s,s')}, \tag{23.16}$$

with a coupling coefficient D_{pb} given by eq. (22.22).

We may interpret the bottom pressure (23.15) as the sum of the surface forcing $\widehat{p}_{2,\mathrm{surf}}$ transmitted to the bottom by ϕ_2, and a direct effect of the Bernoulli head at the bottom which is an additional forcing $\widehat{p}_{2,\mathrm{bot}}$ that partly cancels $\widehat{p}_{2,\mathrm{surf}}$.

We shall see in the next section that the forcing term for seismic noise is $\widehat{p}_{2,\mathrm{surf}} + \cos(lh)\widehat{p}_{2,\mathrm{bot}}$, with $l \leq K \ll k$ the vertical wavenumber in the water. For shallow water gravity waves, $kh \ll 1$ and thus $\cos(lh) \simeq 1$ so that the effective forcing term becomes $\widehat{p}_{2,\mathrm{surf}} + \widehat{p}_{2,\mathrm{bot}}$, which equals the bottom pressure in the incompressible limit. The shallow water asymptote of the spectrum of this total forcing term is very different from the surface pressure only. Compared to eq. (23.22), the $\left[1 + 0.25/\sinh^2(kh)\right]^2$ factor is now replaced by 1. For $kh \ll 1$, this is a factor $(kh)^4/16$ smaller,

For the generation of seismic waves, the only relevant interactions are the ones with phase speeds $|\mathbf{k}+\mathbf{k}'|/|s\sigma+s'\sigma'|$ close to the horizontal speed of seismic modes, typically more than 1500 m/s, except for waves over unconsolidated sediments for which the speed could be only a few hunder meter per second. This condition imposes that $\mathbf{k} \simeq -\mathbf{k}'$ and thus $s\sigma \simeq s'\sigma'$, we can thus ignore the other terms and we re-write eq. (22.17) as

$$\begin{aligned}
\widehat{p}_2 &\simeq -\rho_w \sum_{\mathbf{k},\mathbf{k}'\simeq-\mathbf{k},s} \left\{ \sigma^2 \left[1 + \frac{1}{\tanh^2(kh)} \right] - \frac{g^2k^2}{2\sigma^2\cosh^2(kh)} \right\} Z^s_{1,\mathbf{k}} Z^s_{1,\mathbf{k}'} \mathrm{e}^{\mathrm{i}\left[(\mathbf{k}+\mathbf{k}')\cdot\mathbf{x}-2s\sigma t\right]} \\
&\simeq -\rho_w \sum_{\mathbf{k},\mathbf{k}'\simeq-\mathbf{k},s} \left\{ \sigma^2 \left[\frac{1}{2} + \frac{3}{2\tanh^2(kh)} \right] \right\} Z^s_{1,\mathbf{k}} Z^s_{1,\mathbf{k}'} \mathrm{e}^{\mathrm{i}\left[(\mathbf{k}+\mathbf{k}')\cdot\mathbf{x}-2s\sigma t\right]}
\end{aligned} \tag{23.17}$$

23.3.3 The elementary interaction: a supersonic wave group

Instead of this complete sum, we first detail the simplest case of interaction, with only two monochromatic wave trains in opposite directions with nearly equal periods. Here we take an example with an amplitude a and period $T_a = 12$ s for the first wave train, with a surface elevation $a\cos(k_a x - \sigma_a t)$ and an amplitude b and a period T_b=11.88 s, with a corresponding elevation $b\cos(k_b x + \sigma_b t)$. In the middle of the oceans, with a depth of 5000 m, these two wave trains are in deep water and the difference of the two wavenumbers is $K = k_b - k_a = 5.2 \times 10^{-4}$ rad/m, corresponding to a wavelength $L = 12$ km, to be compared to the wavelength of the first wave tran that is only 225 m. We thus have wave groups that contain 12000/225 = 53 waves (figure 23.4). The group speed is $L \times (1/T_a + 1/T_b)$, namely 2 km/s.

because k in eq. (23.17) can be either k_a or $-k_b$, the equivalent wave-induced pressure has 8 different terms. Only 4 of these terms are relevant for seismic wave generation. We have $Z^+_{1,a} = Z^-_{1,a} = a/2$ and $Z^+_{1,b} = Z^-_{1,b} = b/2$, giving

$$\begin{aligned}
\widehat{p}_2 &\simeq -2\rho_w\sigma^2\frac{ab}{4}\left[\mathrm{e}^{\mathrm{i}[(k_a-k_b)x-2\sigma t]} + \mathrm{e}^{\mathrm{i}[(-k_b+k_a)x-2\sigma t]} + \mathrm{e}^{\mathrm{i}[(k_a-k_b)x+2\sigma t]} + \mathrm{e}^{\mathrm{i}[(-k_b+k_a)x+2\sigma t]}\right] \\
&\simeq -2\rho_w\sigma^2 ab\left[\cos\left(Kx + 2\sigma t\right)\right]
\end{aligned}$$

This result, given by Ardhuin and Herbers (2013) is the generalization to of the Longuet-Higgins (1950) standing wave. The wave group propagates in the direction of the shortest of the two wave components. This propagation in one dimension is easy to generalize to cases where the wave directions are not exactly opposite but in the directions of two wave vectors $\mathbf{k}_b$ and $\mathbf{k}_a$. The direction of propagation of the second order pressure is in the direction of $\mathbf{K} = \mathbf{k}_b - \mathbf{k}_a$. In the incompressible case, this equivalent pressure is equal to the measured pressure in the water column. In reality, with compressibility we have to solve the equations of motion forced by this surface term, this is done in the following sections.

It is also interesting to consider the pressure at the bottom. Indeed, for finite values of kD the orbital velocity at the bottom induces a pressure oscillation given by the usual Bernoulli term, that is equal to $-(u^2+w^2)/2$, which is out of phase with the surface wave groups, whereas $\widehat{p}_2$ is in phase. As noted by Ardhuin and Herbers (2013), these two terms exactly cancel in the limit $kD \to 0$, which is clear from the incompressible solution for the bottom pressure given by Herbers and Guza (1991).

23.3.4 Sum for a continuous spectrum

In the limit of a continuous spectrum, $2\left|Z^+_{1,\mathbf{k}}\right|^2 \to E(k_x,k_y)\mathrm{d}k_x\mathrm{d}k_y$. The factor 2 is there because we use only positive frequencies (i.e. single-sided spectra), namely we gather the variance of the components

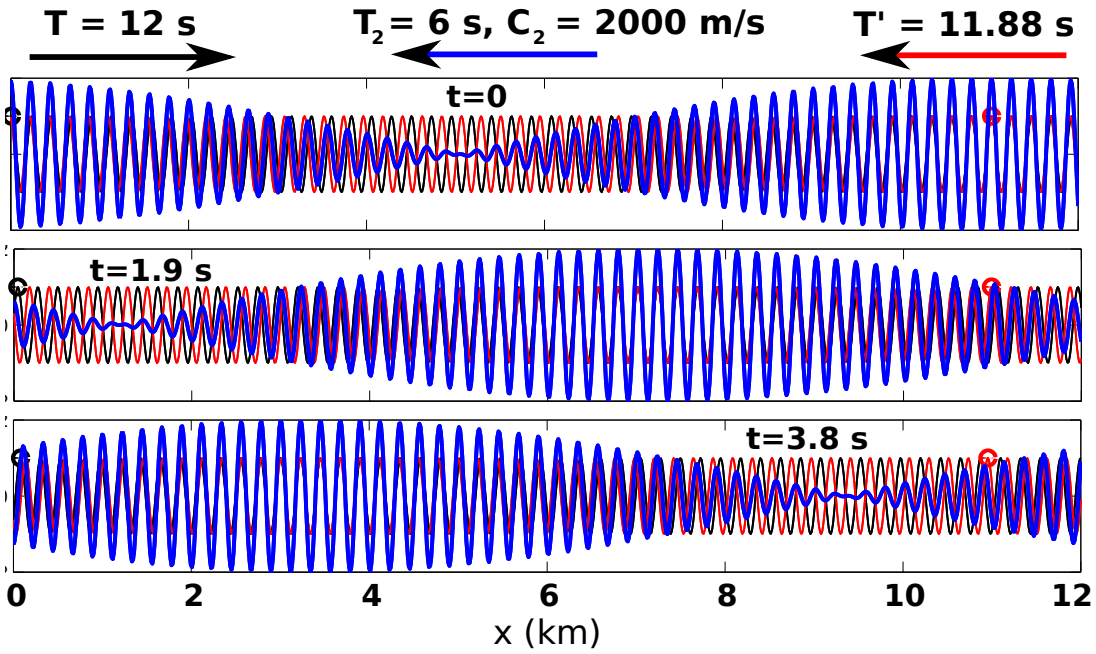

Figure 23.4: Two wave trains with slightly different periods and propagating in opposite directions in deep water interfere to form wave groups. The groups propagate in the same direction as the wave train which has the shorter wave periods. The red and black dots are attached to a crest of their monochromatic component, and these crests travel 100 times slower than the group.

with amplitudes $Z^{+}_{1,\mathbf{k}}$ and $Z^{-}_{1,-\mathbf{k}}$. Liekwise the spectrum of $\widehat{p}_2$ is,

$$F_{p2}(\mathbf{K}, f_s) = 2 \lim_{|d\mathbf{K}|\to 0, df_s \to 0} \frac{|\widehat{p}_2(\mathbf{K}, f_s)|^2}{\mathrm{d}k_{2x}\mathrm{d}k_{2y}\mathrm{d}f_s}, \tag{23.18}$$

where $\widehat{p}_2(\mathbf{K}, f_s)$ is the Fourier amplitude of $\widehat{p}_2$ with wavenumber vector $\mathbf{K}$ and frequency f_s. We now replace with eq. (23.17), and transform the ocean wave spectral density $E(k_x, k_y) = C_g E(f)/(2\pi k)$. Now using $f_s = 2f$, we get $\mathrm{d}k_x\mathrm{d}k_y/\mathrm{d}f_2 = \pi k/C_g \mathrm{d}\theta$ et il vient,

$$F_{p2}(\mathbf{K}, f_s) \simeq 2\rho_w^2\sigma^4 \left[\frac{1}{2} + \frac{3}{2\tanh^2(kD)}\right]^2 \int_{k_x,k_y>0} E(k_x,k_y)E(-k_x+k_{2x},-k_y+k_{2y})\frac{\mathrm{d}k_x\mathrm{d}k_y}{\mathrm{d}f_s} \tag{23.19}$$

$$\simeq 2\rho_w^2 g^2 k^2 \tanh^2(kh) \left[\frac{1}{2} + \frac{3}{2\tanh^2(kD)}\right]^2 \int_{k_x,k_y>0} E(f,\theta)E(f,\theta+\pi)\frac{C_g^2\mathrm{d}k_x\mathrm{d}k_y}{k^2 4\pi^2 \mathrm{d}f_s} \tag{23.20}$$

$$\simeq \rho_w^2 g^2 \tanh^2(kD)\frac{kC_g}{2\pi}\left[\frac{1}{2} + \frac{3}{2\tanh^2(kD)}\right]^2 \int_0^{\pi} E(f,\theta)E(f,\theta+\pi)\mathrm{d}\theta \tag{23.21}$$

$$\simeq \rho_w^2 g^2 \tanh^2(kD) f_s \left(\frac{1}{4} + \frac{kD}{2\sinh(2kD)}\right)\left[\frac{1}{2} + \frac{3}{2\tanh^2(kD)}\right]^2 \int_0^{\pi} E(f,\theta)E(f,\theta+\pi)\mathrm{d}\theta \tag{23.22}$$

In the limit of deep water ($kD \gg 1$), and writing the directional wave spectrum as $E(f,\theta) = E(f)M(f,\theta)$, this becomes

$$F_{p2}(\mathbf{K} \simeq 0, f_s) = \rho_w^2 g^2 f_s E^2(f) I(f)/2, \tag{23.23}$$

where the 'overlap intergral' I was defined by Farrell and Munk (2008) as

$$I(f) = \int_0^{2\pi} M(f,\theta)M(f,\theta+\pi)\mathrm{d}\theta. \tag{23.24}$$

As a result, there are seismic waves generated at all frequencies, provided that some energy travels in opposite directions. This is also true for capillary waves, although in that case the dispersion relation and surface boundary conditions are different (Farrell and Munk, 2008). From an ocean wave perspective,K

is so small compared to k that we can use $K = 0$. However, for the seismic waves, the magnitude and direction of K will determine the type of seismic wave and its direction. Indeed, $K = 0$ correspond to P-waves than travel along the vertical. Because the spectrum F_{p2} is nearly constant for seismic wavenumbers, all the different waves are actually generated at the same time from the same pressure force. In this sense, the wave-induced forcing is equivalent to an oscillating point force at the sea surface.

23.3.5 Free solutions: Rayleigh waves

Motion in the water layer

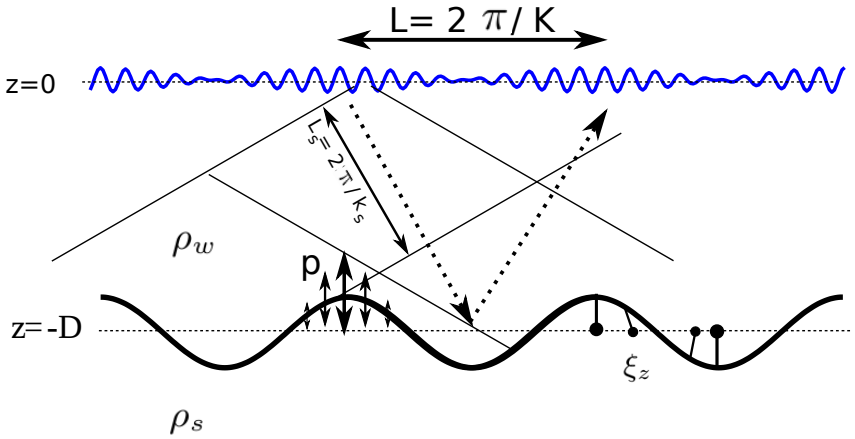

Figure 23.5: Schematic of wave group forcing acoustic waves in a water layer over a solid half-space. The horizontal wavenumber K is set by the forcing, whereas the true acoustic wavelength also involve the vertical component $L_s = 2\pi/k_s = 2\pi/\sqrt{K^2 + l_a^2} = \alpha_w/T$. The dashed arrows give the propagation direction of acoustic waves in the water with the thin solid lines representing the surface of equal phase. The superposition of up-going and down-going waves is a horizontally propagating mode. In practice the angle of propagation of sound waves in Rayleigh modes is less than 65 degrees, as shown in figure 23.7.

For a monochromatic wave of phase $\Theta = Kx - \omega t$, the velocity potential is the real part of

$$\phi = C\mathrm{e}^{l_a(z+h)}\mathrm{e}^{\mathrm{i}\Theta}. \tag{23.25}$$

with l_a a complex vertical wavenumber. Replacing this solution in eq. (23.12) gives

$$-\omega^2 + \alpha_w^2\left(-K^2 + l_a^2 - \frac{g}{\alpha_w^2}l_a\right) \quad = \quad 0 \tag{23.26}$$

with a solution

$$l_a = \frac{g}{2\alpha_w^2} \pm l. \tag{23.27}$$

The water motion is thus a superposition of two terms with the two possible signs,

$$l = \sqrt{\frac{\omega^2}{\alpha_w^2} - K^2 + \frac{g^2}{4\alpha_w^4}} \simeq \sqrt{\frac{\omega^2}{\alpha_w^2} - K^2} \tag{23.28}$$

giving

$$\phi = \mathrm{e}^{gz/2\alpha_w^2}\left(C\mathrm{e}^{il(z+h)} + D\mathrm{e}^{-il(z+h)}\right)\mathrm{e}^{\mathrm{i}\Theta} \tag{23.29}$$

In the ocean $\alpha_w \simeq 1500$ m/s and $z > -11000$ m, so that the term $gz/2\alpha_w$ varies between 0 et 0.02, and can be neglected for simplicity. For a supersonic forcing ($\omega/K > \alpha_w$) l is real and we get acoustic waves, whereas a sub-sonic forcing ($\omega/K < \alpha_w$) gives evanescent waves, decreasing exponential from the sea surface. These are acoustic-gravity modes.

Motion in the solid Earth

Treating the solid Earth as a homogenous medium with a compression velocity α_s and shear velocity β, given by the Lamé coefficients of the solid,

$$\alpha_s^2 = \frac{\lambda+2\mu}{\rho_s}, \tag{23.30}$$

$$\beta^2 = \frac{\mu}{\rho_s}. \tag{23.31}$$

The elasticity equation gives Laplace's equation for the velocity potential ϕ_s and the stream function ψ. With the same phase as in the water, $\Theta = kx - \omega t$ a finite amplitude at $z \to -\infty$ gives solutions of the form

$$\phi_s = A\mathrm{e}^{m(z+h)}\mathrm{e}^{\mathrm{i}\Theta}, \tag{23.32}$$

$$\psi = B\mathrm{e}^{n(z+h)}\mathrm{e}^{\mathrm{i}\Theta}. \tag{23.33}$$

The vertical wavenumbers m and n are given by the generalized Bernoulli equation,

$$m = \frac{\mathrm{i}g}{2\alpha_s} + \sqrt{K^2 - \frac{\omega^2}{\alpha_s^2} - \frac{g^2}{4\alpha_s^2}} \simeq \sqrt{K^2 - \frac{\omega^2}{\alpha_s^2}} \quad \text{and} \quad n \simeq \sqrt{K^2 - \frac{\omega^2}{\beta^2}}, \tag{23.34}$$

where A and B are the two constant amplitudes of the velocity potential and streamfuction, that have units of m^2/s. These two unknowns are given by the boundary conditons.

Hence, the horizontal and vertical displacements are given by the real parts of

$$\xi_x = \left(KA\mathrm{e}^{m(z+h)} + \mathrm{i}nB\mathrm{e}^{n(z+h)}\right)\mathrm{e}^{\mathrm{i}\Theta}/\omega, \tag{23.35}$$

$$\xi_z = \left(-\mathrm{i}mA\mathrm{e}^{m(z+h)} + KB\mathrm{e}^{n(z+h)}\right)\mathrm{e}^{\mathrm{i}\Theta}/\omega \tag{23.36}$$

The first term is a compression wave with a velocity field $u_A = \partial\xi_x/\partial t = \partial\phi_s/\partial x$, avec $\phi_s = A\mathrm{e}^{m(z+h)}\mathrm{e}^{\mathrm{i}\Theta}$. The second term is a shear wave with a velocity field $u_B = \partial\xi_x/\partial t = -\partial\psi/\partial z$.

Coupling at the water-solid interface requires to express the stresses in the solid using Hooke's law, which states that the stress is linearly related to the strain,

$$\tau_{zz} = \lambda\left(\frac{\partial\xi_x}{\partial x} + \frac{\partial\xi_z}{\partial z}\right) + 2\mu\frac{\partial\xi_z}{\partial z}, \tag{23.37}$$

$$\tau_{xz} = \mu\left(\frac{\partial\xi_x}{\partial z} + \frac{\partial\xi_z}{\partial x}\right). \tag{23.38}$$

In our case we consider that the water freely slips over the solid, so that the shear stress at the bottom is $\tau_{xz} = 0$ at $z = -h$. Using (23.35)–(23.36) we get,

$$B = \frac{2\mathrm{i}Km}{n^2+K^2}A. \tag{23.39}$$

This relationship is characteristic of Rayleigh waves.

Coupling of water and solid Earth and pseudo-Rayleigh waves

The boundary condtions $w_+ = w_-$ and $\tau_{zz} + p = 0$ give the following relations that couple the amplitudes A, C and D,

$$A(m - \frac{2K^2m}{n^2+K^2}) - \mathrm{i}lE + \mathrm{i}lF = 0, \tag{23.40}$$

$$A\frac{\mathrm{i}}{\omega}\left[-\rho_s m^2\alpha_s^2 + \lambda K^2 + 4\mu\frac{K^2mn}{n^2+K^2}\right] - \mathrm{i}\omega\rho_w E - \mathrm{i}\omega\rho_w F = 0. \tag{23.41}$$

Replacing λ and μ by their expression in terms of α_s and β, this gives

$$A\frac{m\omega^2}{\omega^2 - 2K^2\beta^2} - \mathrm{i}lE + \mathrm{i}lF = 0, \tag{23.42}$$

$$A\frac{\mathrm{i}}{\omega\beta^2}\rho_s\left[-\frac{4\beta^4K^2mn}{\omega^2-2K^2\beta^2} + \left(\omega^2 - 2K^2\beta^2\right)\right] - \mathrm{i}\omega\rho_w E - \mathrm{i}\omega\rho_w F = 0 \tag{23.43}$$

The last unknown, ω is now given by the sea surface boundary condition. Without forcing, this is $p(z=\zeta)=0\simeq p(z=0)$, and it gives,

$$E = B_2 \mathrm{e}^{-ilh}, \tag{23.44}$$
$$F = -B_2 \mathrm{e}^{ilh}, \tag{23.45}$$

and

$$\frac{m\omega^2}{\omega^2 - 2K^2\beta^2} A - 2il\cos(lh)B_2 = 0 \tag{23.46}$$
$$\frac{\mathrm{i}}{\omega\beta^2}\rho_s \left[-\frac{4\beta^4 K^2 mn}{\omega^2 - 2K^2\beta^2} + \left(\omega^2 - 2K^2\beta^2\right) \right] A - 2\omega\rho_w \sin(lh)_2 B = 0. \tag{23.47}$$

The determinant of this linear system is thus zero, which gives the dispersion relation first given by Stoneley (1926),

$$\tan(lh) = \frac{\rho_s}{\rho_w}\frac{l}{m} \times \frac{4\beta^4 K^2 mn - \left(\omega^2 - 2K^2\beta^2\right)^2}{\omega^4}. \tag{23.48}$$

We also have

$$B_2 = m\frac{(n^2+K^2) - 2K^2}{(n^2+K^2)\,(2il\cos(lh))} A = m\mathrm{i}\frac{\omega^2}{(2K^2\beta^2 - \omega^2)2l\cos(lh)} A. \tag{23.49}$$

The dispersion relation (23.48) and motion are characteristic of Rayleigh waves, modified by a water layer. Because of this modification, these are usually called pseudo-Rayleigh waves.

The practical use of the dispersion relation is complicated by the presence of multiple solutions that are associated with different modes,

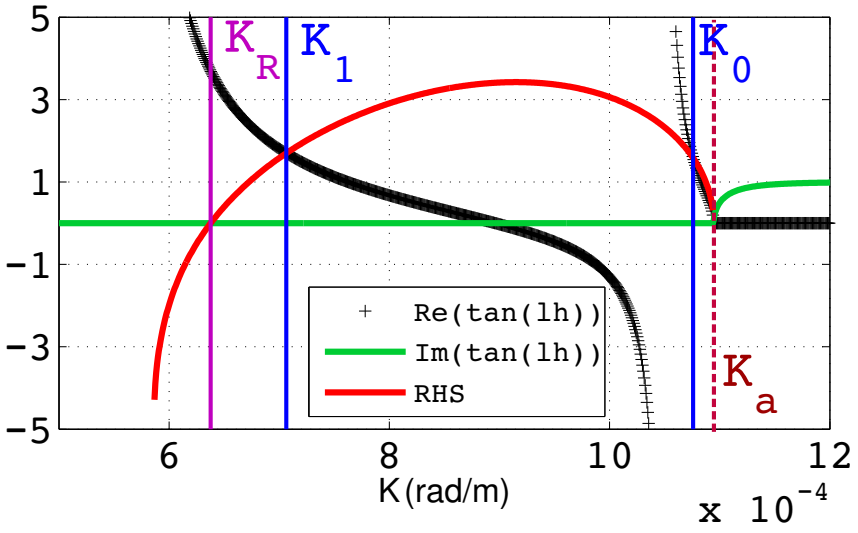

Figure 23.6: Real and imaginary parts of the left hand side and real part of the right hand side of eq. 23.48. This calculation was performed for a water depth $D = 5000$ m, with a sound speed in water of $\alpha_w = 1500$ m/s, a shear wave speed of $\beta = 2800$m/s and water and crust densities of 1000 et 2500 kg/m^3. The chosen seismic frequency is $f_s = 0.263$ Hz, corresponding to a non-dimensional depth $f_s h/\alpha_w = 0.88$. The determinant of the system is zero for three values: one acoustic mode K_a for which $l = 0$ (horizontal propagation) and two seismic Rayleigh modes with wavenumbers K_0 and K_1. For non-dimensional frequencies below 0.34, only the 0 mode exists, and as the frequency increases, K_0 increases and new branches of $\tan(lh)$ appear (in black) giving higher modes, that have a lower value of K. Besides, the zero of the right hand side (in red) gives the wavenumber of Rayleigh waves K_R in the absence of a water layer.

Figure 23.6 shows how different values of K are possible due to the multiple branches of the tangent function.

The dispersion relation 23.48 is slightly different from that of Rayleigh waves without an ocean layer, which is

$$\beta^4 K^2 mn - \left(\omega^2 - 2K^2\beta^2\right)^2 = 0. \tag{23.50}$$

We also note that for large depths or short wavelengths ($lh > 3\pi/2$) there are several solutions that correspond to different modes, each with a distinct motion pattern in the water column, while the pattern in the crust remains similar. Figure 23.7 shows the phase speed that are between the sound speed and the shear wave speed. For a given mode, the higher the frequency, the slower the horizontal propagation which tends to the sound speed. The acoustic part in the water thus propagate at shallower angles, becoming horizontal in the limit of high frequency.

For high enough frequencies, the acoustic wavelength is much shorter than the water depth, and the variation in sound speed across the water layer can modify the propagation. In particular, nearly horizontal sound waves can be trapped in the SOFAR channel, and there can be a decoupling of the water layer and solid Earth.

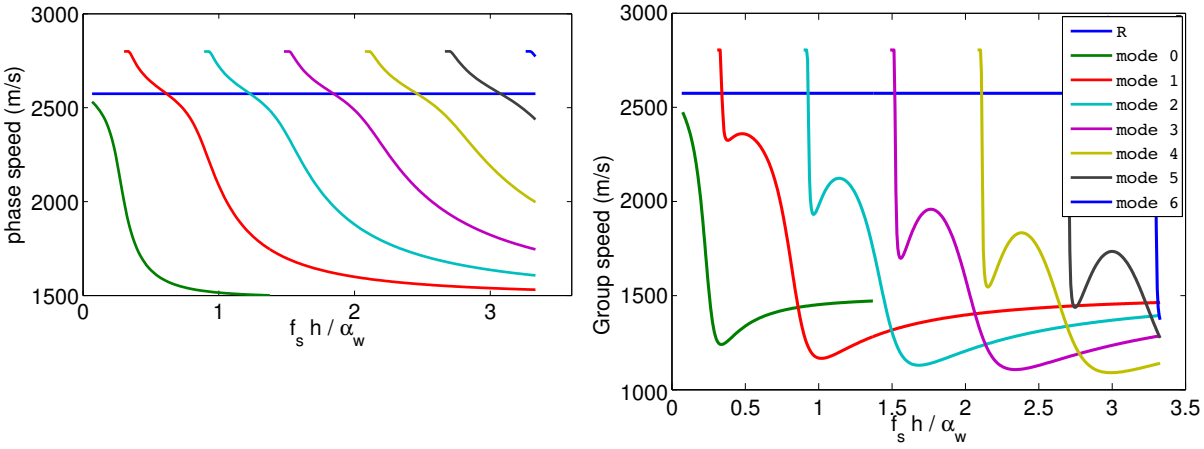

Figure 23.7: Phase speeds and group speeds for Rayleigh waves in the presence of a water layer. Calculations have been made with a water depth $D = 5000$ m, a sound speed in the water $\alpha_w = 1500$ m/s, a shear wave speed of $\beta = 2800$m/s and water and crust densities of 1000 et 2500 kg/m^3. Without the water layer the values are given by the blue line: in that case the Rayleigh waves are not dispersive. We have used seismic frequencies from 0 to 1 Hz, the latter value corresponding to $f_s h/\alpha_w = 3.4$.

The angle of the acoustic propagation in the water are plotted for $D = 5000$ m in figure 23.8, together with the vertical profiles of velocities in the water and crust. We note that the higher modes, with a lower K, penetrate deeper in the solid Earth.

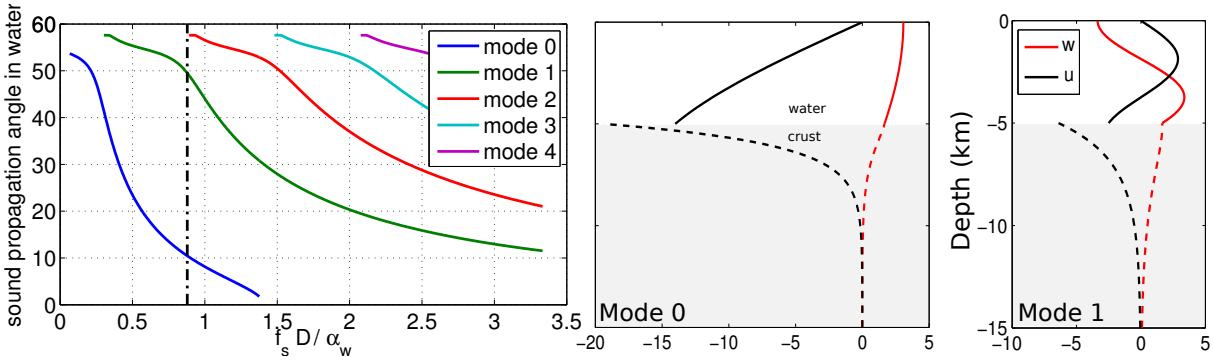

Figure 23.8: (a) Angle of propagation, relative to the hoizontal, of the two acoustic waves that combine to make acoustic modes in the water. The vertical profile of the velocity amplitude for mode 0 and 1 and $f_s D/\alpha_w = 0.88$ are shown in the right panels. For modes 1 and higher, the vertical velocity is zero at the nodes of the vertical standing acoustic wave. The zero-pressure level correspond to the zero-velocity levels, in particular at the surface.

Displacements, pressure, velocity and energy in Rayleigh waves

To finish with this description of Rayleigh waves, we can express all the wave-related quantities in terms of the ground displacement amplitude at the top of the crust δ,

$$\begin{aligned}
A &= \frac{\omega^2 - 2k^2\beta^2}{m\omega^2}\delta && (23.51)\\
B &= \frac{2\mathrm{i}km}{n^2+K^2}A && (23.52)\\
B_2 &= \frac{\mathrm{i}\omega}{2l\cos(lD)}\delta && (23.53)\\
\xi_z(z=-D) &= \delta\cos\Theta && (23.54)\\
\phi_s &= A\mathrm{e}^{m(z+D)}\mathrm{e}^{\mathrm{i}\Theta} && (23.55)\\
\psi &= B\mathrm{e}^{n(z+D)}\mathrm{e}^{\mathrm{i}\Theta} && (23.56)\\
\phi &= 2\mathrm{i}lB_2\sin(lz)\mathrm{e}^{\mathrm{i}\Theta} && (23.57)\\
p'(z) &= \mathcal{R}\left[\mathrm{i}\rho_w\omega\phi\right] = -\delta\rho_w\omega^2\frac{\sin(lz)}{l\cos(lD)}\cos\Theta. && (23.58)
\end{aligned}$$

From these we can evaluate the seismic wave energy per unit horizontal surface E_s, taking twice the kinetic energy in both water and solid Earth,

$$\begin{aligned}
E_s &= \rho_w\int_{-D}^{0}\overline{(u^2+w^2)}\mathrm{d}z + \rho_s\int_{-\infty}^{-D}\overline{(u^2+w^2)}\mathrm{d}z && (23.59)\\
&= T_{E\delta}(D)\frac{\delta^2}{2} \quad \text{with} && (23.60)\\
T_{E\delta}(D) &= \rho_s\left[\frac{(KB/A+m)^2}{2m}+\frac{(nB/A+K)^2}{2n}\right]\left(\frac{A}{\delta}\right)^2\\
&\quad +\rho_w\left\{l^2\left[2D+sin(2lD)/l\right]+K^2\left[2D-sin(2lD)/l\right]\right\}\left(\frac{B_2}{\delta}\right)^2 && (23.61)
\end{aligned}$$

23.4 Forced solutions: Acoustic-Gravity, Rayleigh and body waves

23.4.1 Matrix inversion

Let us now consider what happens with the ocean wave forcing. The surface boundary condition is now $p' = P\mathrm{e}^{\mathrm{i}(Kx-\omega t)}$ at $z=0$, and $p' = -\rho_w\partial\phi_2/\partial t + P_b\mathrm{e}^{\mathrm{i}(Kx-\omega t)}$ at the bottom. This is now analog to the problem of wave generation by the wind, treated in chapter **??**.

Boundary conditions are now, for $kD \gg 1$, and neglect P_b,

$$\begin{aligned}
E\mathrm{e}^{ilh} + F\mathrm{e}^{-ilh} &= \frac{\mathrm{i}P}{\rho_w\omega} && (23.62)\\
\frac{m\omega^2}{\omega^2-2k^2\beta^2}A - \mathrm{i}lE + \mathrm{i}lF &= 0 && (23.63)\\
\frac{-\rho_s}{\omega^2\rho_w}\left[-\frac{4\beta^4k^2mn}{\omega^2-2k^2\beta^2}+\left(\omega^2-2k^2\beta^2\right)\right]A + E + F &= 0 && (23.64)
\end{aligned}$$

or, in matrix form,

$$M\begin{pmatrix}A\\E\\F\end{pmatrix} = \frac{\mathrm{i}}{\rho_w\omega}\begin{pmatrix}P\\0\\0\end{pmatrix} \qquad (23.65)$$

The solution of this system of equation is the sum of a the solutions to the 'homogenous system' (without forcing) and one particular solution with the forcing. That solution can be written using the

determinant and co-factors od the matrix [1] M giving

$$A = -2li P/\det M \tag{23.68}$$

with

$$\det M = \frac{2}{\omega\left(\omega^2 - 2K^2\beta^2\right)}\left\{l\rho_s \cos(lD)\left[4\beta^4 k^2 mn - \left(\omega^2 - 2K^2\beta^2\right)^2\right] - \rho_w m \sin(lD)\omega^4\right\}. \tag{23.69}$$

23.4.2 Four different types of waves and equivalent point force

The amplitude of the seismic displacement as a function of the sea surface pressure amplitude in the form of a gain factor $\delta = G(\omega)P(\omega)$, with the gain

$$G = \frac{2lm(K^2 - n^2)}{(n^2 + K^2)\omega \det M}. \tag{23.70}$$

Contrary to the case without forcing, we can now have waves at all wavenumbers and frequencies, but their amplitude GP varies as shown in figure 23.9. We can distinguish 4 different domains

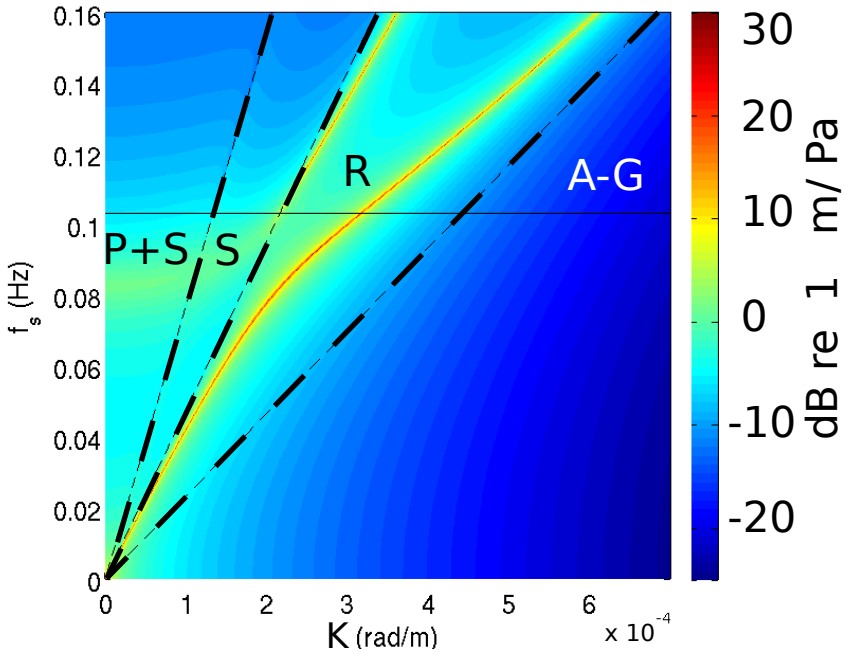

Figure 23.9: Magnitude of the transfer function $G(K, f_s)$ illustrating the singularities along the dispersion relations of the free Rayleigh modes with wavenumbers $K = K_n(f_s)$, that correspond to $\det(M) = 0$. The oblique dashed lines correspond to phase speeds equal to α_c, β, and α_w, and separate the four domains body waves (P+S), mixed body and evanescent waves (S), Rayleigh waves (R) and acoustic-gravity modes (A-G).

- acoustic-gravity waves (AG) for $K/\omega < \alpha_w$: for a monochromatic forcing, these waves vanish exponentially with depth
- free and forced Rayleigh waves for $\alpha_w < K/\omega < \beta$: the free waves are the ones with $\omega = \omega_r$
- evanescent P waves and SV body waves for $\alpha_s < K/\omega < \beta$: the SV propagate down in the solid Earth

[1] For a linear system of three equations

$$\begin{pmatrix} a & b & c \\ d & e & f \\ g & h & i \end{pmatrix}\begin{pmatrix} A \\ E \\ F \end{pmatrix} = \begin{pmatrix} 1 \\ 0 \\ 0 \end{pmatrix}, \tag{23.66}$$

the determinant is

$$\det M = aei + bfg + cdh - ceg - fha - ibd \tag{23.67}$$

and the first co-factor is $ei - fh$ so that $A = (ei - fh)/\det M$, and likewise $E = (fg - di)/\det M$ and $F = (dh - eg)/\det M$.

- P and SV body waves for $\alpha_s > K/\omega$: both P and SV propagate down in the solid Earth.

Ocean waves are random and have a spectrum with a finite width which is typically much wider than the K's of Rayleigh waves, so that waves at a given location excite, simultaneously, a broad range of wave numbers on the wavenumber plane, ans illustrated by figure 23.10. The wave-induced pressure spectrum

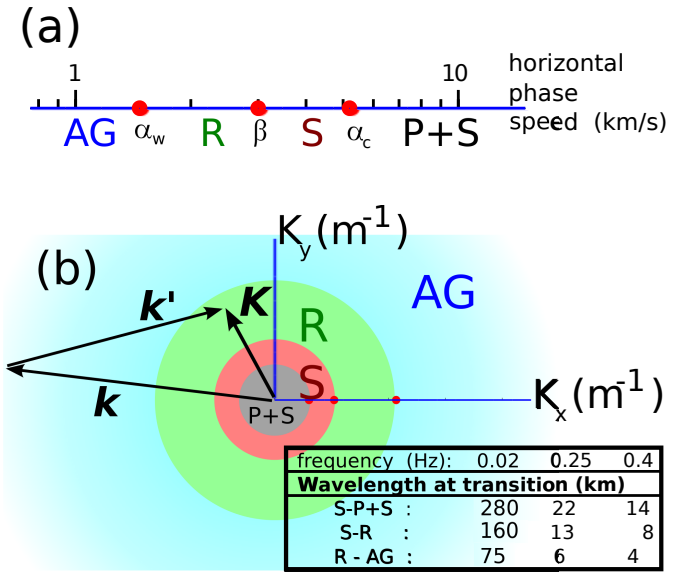

Figure 23.10: (a) The vertical evanescent or propagating nature of the noise field in the solid and liquid layers is defined by the horizontal phase speeds relative to the distinct values of the sound speed in the ocean (α_w), and the shear (β) and compression (α_c) speeds in the crust. From slow to fast, there are the acoustic-gravity (AG) domain, the Rayleigh (R) wave domain, and two body wave domains (S only, and P and S together) (b) For any fixed frequency, the four domains correspond to 4 concentric regions in the wavenumber plane. For three selected noise frequencies generated by OSGW in the infragravity, dominant and high frequency ranges of the forcing wave field, the limiting wavelengths between the four domains are indicated, using $\alpha_w = 1.5$ km/s, $\beta = 3.2$ km/s, $\alpha_c = 5.54$ km/s. One example of interaction is shown with two gravity wave modes that interact to generate a Rayleigh wave (black vectors, not to scale, k and k' should be much larger).

$F_p(K_x, K_y, f_s)$ waries smoothly around $K = 0$ and is roughly constant for seismic wavenumbers. Thus, it is simimar to a white spectrum, corresponding to the spectrum of delta function in horizontal (x, y) space. Hence, in terms of the power spectrum of the radiated waves, the ocean wavemotion is equivalent to a vertical oscillating force pushing on a single point of the sea surface with a root mean square value,

$$F_{\rm rms} = 2\pi\sqrt{F_p(K_x = 0, K_y = 0, f_s) dA df_s}, \tag{23.71}$$

where dA is the area over which the forcing is distributed and df_s is the frequency interval of interest. This equivalence is easy to show by computing the spectrum in K_x, Ky of such a force, either directly as a delta function or as a pressure over a small square and taking the size of that square to zero. The spectrum of that force is equal to $F_p(K_x = 0, K_y = 0, f_s)$ for all values of K_x and K_y, unlique the true effect of waves which becomes zero for large K. Also, compared to this point force, the phases of the different seismic modes are independant with real waves whereas they are identical with the point force. As a result, correlations of synthetic traces from a model forced by such point forces may be artificially high, where as power spectral densities should be alright. Such vertical forces were used by Gualtieri et al. (2013) to model the seismic response, which contains all four types of waves, AG, R, P and S. We will now discuss these 4 types of waves.

23.4.3 Rayleigh waves

For a given wavenumber K, there are one or several values of ω that gives a zero determinant, for which G is infinite. Let us call ω_r one of these values, ω_r and K are related by the Rayleigh wave dispersion relation (23.48). In practice the wave forcing is continuous across frequencies and wavenumbers and

characterized by a power spectral density $F_p(K_x, K_y, f)$, and in the case of the double-frequency source it is $F_{p2}(K_x, K_y, f)$ given by eq. (23.22). It is thus possible to find the power spectrum of the ground displacement by integrating in frequency across these singularities,

$$F_\delta(K_x, K_y) = \int_0^\infty |G|^2 F_{p3D}(K_x, K_y, \omega) \mathrm{d}\omega \tag{23.72}$$

or in terms of seismic energy

$$F_E(K_x, K_y) = T_{E\delta}(D) F_\delta(K_x, K_y) \tag{23.73}$$

with $T_{E\delta}(D)$ given by (23.61).

Where the singularities in G can be expanded at $G = G'(\omega)/(\omega^2 - \omega_r^2)$. Following Hasselmann (1962)it is easy to prove that the response of a harmonic oscillator forced by a continuous spectrum of density $F_p K_x, K_y, \omega$ with a singularity at $\omega = \omega_r$ integrates to a finite spectral density that grows linearly in time, giving a rate of change,

$$\frac{\partial F_\delta(k_x, k_y)}{\partial t} = S_{DF}(k_x, k_y) = \frac{\pi |G'|^2}{2\omega_r^2} F_p(k_x, k_y, \omega_r). \tag{23.74}$$

In practice we are often in a situation where the wave field changes slowly at the time scale of seismic propagation. In this quasi-stationary situation, assuming seismic energy conservation along rays, we have an energy balance similar to that of ocean waves, with conservation of the spectral densities in $K-$space,

$$\mathbf{U} \cdot \boldsymbol{\nabla} F_E(K_x, K_y) = T_{E\delta}(h) S_{DF}(k_x, k_y), \tag{23.75}$$

where U is the group speed of seismic waves. The seismic spectrum at point $s = 0$ is given by the integral of sources along propagation rays with an along-ray distance s. Introducing the dissipation of seismic waves by anelastic processes, represented by a non-dimensional factor Q, we have

$$F_{\delta,0}(K_x, K_y)(K_x(0), K_y(0)) = \int_O^\infty \frac{T_{E\delta}(s)}{T_{E\delta}(0)} \frac{S_{DF}(K_s(s), K_y(s))}{U(s)} \exp\left[- \int_0^{s'} \frac{\omega}{U(s')Q(s')} \mathrm{d}s' \right] \mathrm{d}s \tag{23.76}$$

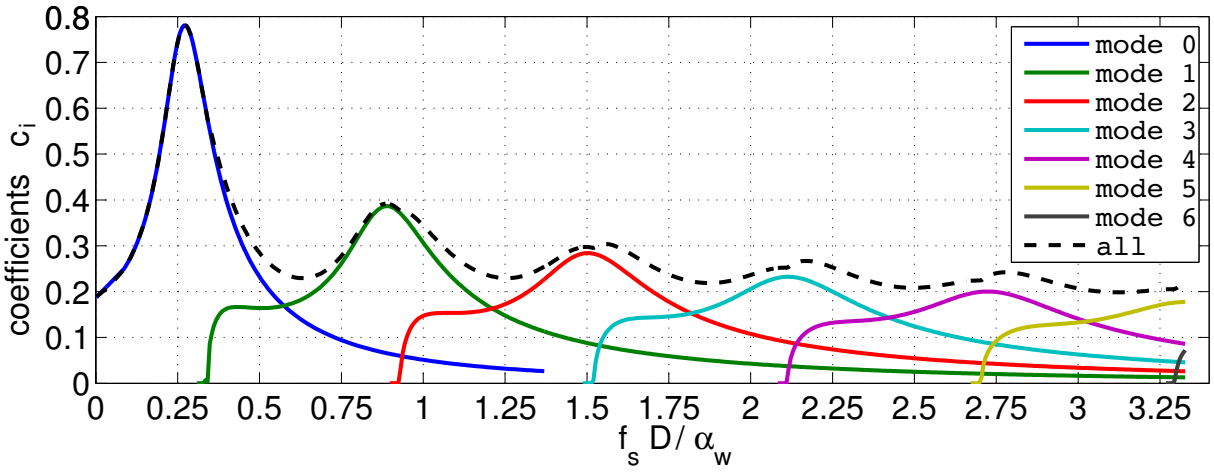

Figure 23.11: Non-dimensional coefficients c_i and $\widetilde{C}$. We note that the peaks of modes $i = 0$ and $i = 1$ occur for depths D that are close to but slightly larger than D $0.25 + i/2$ the acoustic wavelength, just like the resonant modes of an oran pipe. In fact c_i is maximum for a depth that is exactly $0.25 + i/2$ the *vertical* wavelength: because the propagation direction is oblique in the water, what is important for a maximum c_i is the constructive interference of these waves that reflect on the bottom and surface. This figure was drawn for $\alpha_w = 1500$ m s^{-1} and $\beta = 2800$ m s^{-1}. The peak of c_0 is higher for larger values of β/α_w, which is similar to the impedance ratio of the bottom that defines the reflection of waves at the bottom. For example, changing β to 3200 m s^{-1}, the maximum value of c_0 is 1.03.

It is more convenient to work in azimuth and frequency because frequency is conserved during propagation. For the Rayleigh mode number i we have

$$F_{\delta,0}(\omega, \theta_s) = \frac{K(0)}{U(0)} F_{\delta,0}(K_x(0), K_y(0)). \tag{23.77}$$

To simplify our equations we will now assume that Q is independent of the distance along the ray s, and we get

$$F_{\delta,0}(\omega,\theta_s) = \int_O^\infty \frac{S_{DF}(\omega)}{U(s)} \exp\left[-\frac{\omega}{Q}t(s)\right] \mathrm{d}s \tag{23.78}$$

where $t(s)$ is the travel time (propagation time) and

$$S_{DF}(\omega) = \frac{k(0)}{U(0)} \frac{T_{E\delta}(s)}{T_{E\delta}(0)} \frac{S_{DF}(k_x,k_y)}{U(s)}. \tag{23.79}$$

This source is a source of the power spectral density of the vertical elevation variance at point 0, per unit propagation length along a seismic ray. It thus has units of distance times time (m s).

Equations are more simple when this source is written per unit propagation distance

$$\begin{aligned} S_{DF}(\omega) &= \frac{K(0)U(s)}{U(0)K(s)} \frac{T_{E\delta}(s)}{T_{E\delta}(0)} \frac{K(s)S_{DF}(K_x,K_y)}{U^2(s)} &(23.80)\\ &= \frac{K(0)U(s)}{U(0)K(s)} \frac{T_{E\delta}(s)}{T_{E\delta}(0)} \frac{2\pi\omega c_i^2}{\beta^5\rho_s^2} F_{p3D}(K_x,K_y,\omega) &(23.81)\end{aligned}$$

where c_i is a non-dimensional coefficent that is a function of the non-dimensional depth $\omega D/\alpha_w$ and the seismic mode index i,

$$c_i = \sqrt{\frac{\beta^5\rho_s^2 k_i}{U_i^2 2\pi\omega} \frac{\pi\left|G_i'\right|^2}{2\omega^2}}. \tag{23.82}$$

Going to an extreme simplification, we will assume that U and K are independant of i and D. The seismic source is thus of the order of

$$S_{DF}(f_s) \simeq \frac{2\pi\omega\widetilde{C}^2}{\beta^5\rho_s^2} F_{p3D}(k_x,k_y,f_s). \tag{23.83}$$

where $\widetilde{C}$ combines all the c_i values

$$\widetilde{C}^2 = \sum_{i=0}^{\infty} c_i^2. \tag{23.84}$$

The values of c_i are obtained by finding the roots of the dispersion relation and using eq. (23.82). This gives values such as given in figure (23.11). When combining all modes the coefficient $\widetilde{C}$ varies with the ration of the vertical acoustic wavelength and the water depth D.

23.4.4 body waves

A first theory of body wave generation by ocean waves was proposed by Vinnik (1973), who found that in some regions far from the ocean, the recorded microseism signals were dominated by body waves and not by surface Rayleigh waves. Since that time, many observations of body waves have been performed (e.g. Zhang et al., 2010; Obrebski et al., 2013). The theory of Vinnik did not include the important effect of the water layer. This was corrected by Ardhuin and Herbers (2013) who simply applied the Hasselmann (1963) theory. This theory can explain both P and SV waves, but not the transversally polarized SH waves observed by Nishida and Takagi (2016), which probably require some bottom slopes or mode conversion. The following theoretical expression for the spectrum of P waves was also derived by Gualtieri et al. (2014), and a first quantitative verification was performed by Farra et al. (2016).

In the case of body waves, for $K/(2\pi f_s) > \beta$, there are no singularities and thus the spectrum of the ground displacement is directly given by,

$$F_{\delta,P}(f_s) = f_s E^2(f) I(f) \frac{\rho_w^2 g^2}{\rho_s^2\beta_s^4} c_P^2 \tag{23.85}$$

with a non-dimensional coefficient c_P,

$$c_P^2 = 2\pi \int_0^{\omega_s/\alpha_c} \frac{4l^2m^2\rho_s^2\beta_s^4}{\omega_s^2 \det^2(M)} K\mathrm{d}K. \tag{23.86}$$

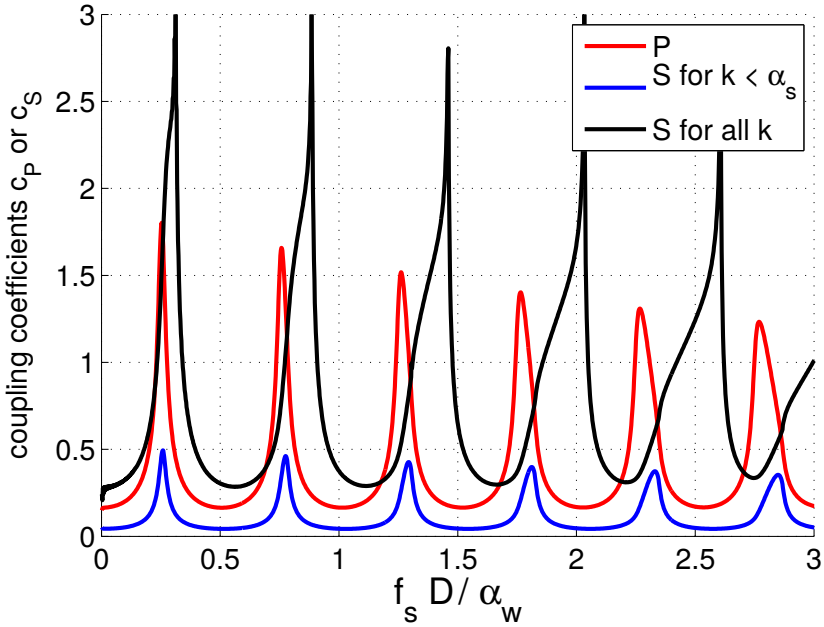

Figure 23.12: Non-dimensionless coefficients c_P and c_S that amplify the wave-induced pressure into ground displacement associated with P and S waves.

A similar expression can be written for S waves, and both are illustrated in figure 23.12,

$$F_{\delta,S}(f_s) = f_s E^2(f) I(f) \frac{\rho_w^2 g^2}{\rho_s^2 \beta_s^4} c_S^2. \tag{23.87}$$

However, in the range of wavenumbers where S waves exist, $k < \omega_s/\beta$, there can also be evanescent P waves, and the system can approach the singularity for $\omega_s = \omega_{s,j}$ and $k = \omega_s/\beta$. We evaluated numerically the coefficient

$$c_S^2 = 2\pi \int_0^{\omega_s/\beta} \frac{4l^2 m^2 k^2 \rho_s^2 \beta_s^4}{\omega_s^2 (n^2 + k^2) \det^2(M)} K \mathrm{d}K. \tag{23.88}$$

It is striking that the maxima of the coefficients c_P and c_S are much more pronounced that that of c_i for Rayleigh waves,shown in figure 23.11. This is probably due the fact that, in the case of P and S waves, the acoustic waves in the water are propagating closer to the vertical, with a narrow range of angles. As a result, the spatial distribution of sources of body waves is much more constrained by the water depth, and should focus on smaller regions (Obrebski et al., 2013).

For the estimation of the spectrum recorded outside of a source area, it is more convenient to express the local seismic source as a function of the horizontal propagation angle θ, and the vertical take-off angle φ. For P waves, this gives,

$$F_{\delta,P}(f_s, \theta, \varphi) = f_s E^2(f) I(f) \frac{1}{\rho_s^2 \beta_s^4} c_{P,\varphi}^2 \sin\varphi \tag{23.89}$$

with the non-dimensional coefficient $c_{P,\varphi}$ defined by

$$c_{P,\varphi}^2 = \frac{4l^2 m^2 \rho_s^2 \beta_s^4}{\omega_s \alpha_c \det^2(M)} \frac{\partial K}{\partial \varphi}, \tag{23.90}$$

which is the normalized source per unit solid angle Ω, so that the average over the half space of downward directions Ω^- is

$$c_P^2 = \int_0^{2\pi} \int_0^{\pi/2} c_{P,\varphi}^2 \sin\varphi \mathrm{d}\varphi \mathrm{d}\theta = \int_{\Omega^-} c_{P,\varphi}^2 \mathrm{d}\Omega \tag{23.91}$$

as defined by eq. (23.86).

It is noteworthy that the distribution of the P-wave energy with the take-off angle is very close to the one given by a small disk pushing at the top of a uniform half space, as given by Miller and Pursey

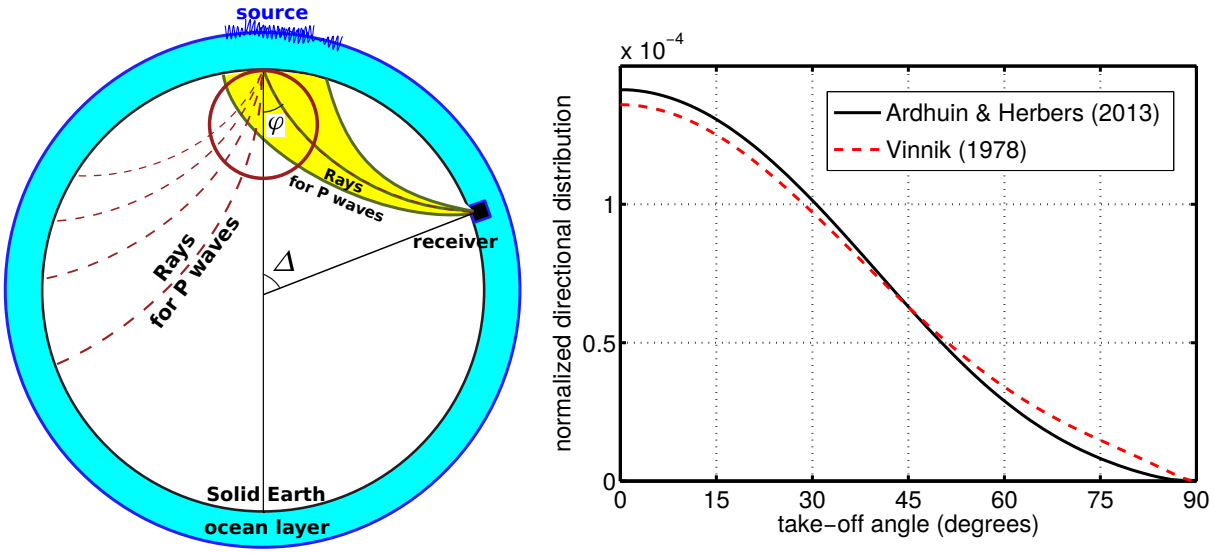

Figure 23.13: Left: schematic of body wave propagation and definitions of take-off angle φ and epicentric angle Δ. Right: Dimensionless coefficients $c_{P,\varphi}$ that amplify the wave-induced pressure into ground displacement. The maximum for a zero take-off angle corresponds to vertically propagating compression waves, and the compression waves that propagate along the crust have a vanishing amplitude.

(1955) and used by Vinnik (1973), although it also varies with the non-dimensional water depth $f_s h/\alpha_w$. The only missing item in the work by Vinnik (1973) is the very strong amplification of the motion for resonant frequencies associated with the water layer. Due to the large impedance contrast at the water-crust interface the relative amplification of P waves is one order of magnitude stronger than for Rayleigh waves. We thus expect a much tighter correspondence of the strong seismic noise sources with the water depths that correspond to a maximum amplification.

Ardhuin and Herbers (2013) estimated that P waves will dominate the signal at large distances from the source. The exact location where P-wave levels overtakes Rayleigh-wave levels depends on the relative attenuation of the two types of waves. With a realistic $Q = 2000$ for the P waves, and $Q = 400$ for the Rayleigh waves, figure 23.14 shows that it occurs at an epicentric angle of $\Delta \simeq 40°$, which is a distance of 4400 km, consistent with the observations reported by Vinnik (1973) using Kazakhstan array data.

23.4.5 acoustic-gravity waves

At the other end of the scale of forcing speeds, for $K/(2\pi f_s) < \alpha_w$, the response in the acoustic-gravity regime is also given by the local forcing.

In order to illustrate the different types of solutions, it is interesting to evaluate the solution for an unbounded ocean, in which sound waves are radiated from the surface only. The velocity field and associated pressure fluctuations are

$$\phi_2 = \frac{1}{\rho_w}\int \frac{\mathrm{i}\omega_s \widehat{p}_2(\mathbf{K}, f_s)}{-\omega_s^2 + \mathrm{i}gl} \mathrm{e}^{\mathrm{i}\left[-lz+\Theta(\mathbf{k},\mathbf{k}',s,s')\right]} \mathrm{d}\mathbf{K}\mathrm{d}f_s \tag{23.92}$$

$$p_2 = \int \frac{\widehat{p}_2(\mathbf{K}, f_s)}{1 - \mathrm{i}gl/\omega_s^2} \mathrm{e}^{\mathrm{i}\left[-lz+\Theta(\mathbf{k},\mathbf{k}',s,s')\right]} \mathrm{d}\mathbf{K}\mathrm{d}f_s \tag{23.93}$$

where p_2 has been obtained using the linearized version of eq. (23.10). The measured pressure signal is the sum of the linear pressure p_1, the second-order wave pressure p_2 given by eq. (23.93), and the Bernoulli correction $p_{2,B}$ given by

$$p_{2,B}(z) = \rho_w \sum_{\mathbf{k},s,\mathbf{k}',s'} D_{pb}\left(\mathbf{k}, s, \mathbf{k}', s', z\right) Z^s_{1,\mathbf{k}} Z^{s'}_{1,\mathbf{k}'} \mathrm{e}^{\mathrm{i}\Theta(\mathbf{k},\mathbf{k}',s,s')}. \tag{23.94}$$

We note that $p_{2,\mathrm{bot}}$ defined in eq. (23.16) is equal to $p_{2,B}(z = -h)$.

We shall neglect $g|l|/\omega_s^2$, which is bounded by the ratio between the deep water gravity and sound speeds, which is less than 0.1 for wave periods less than 180 s. We express the velocity potential as a

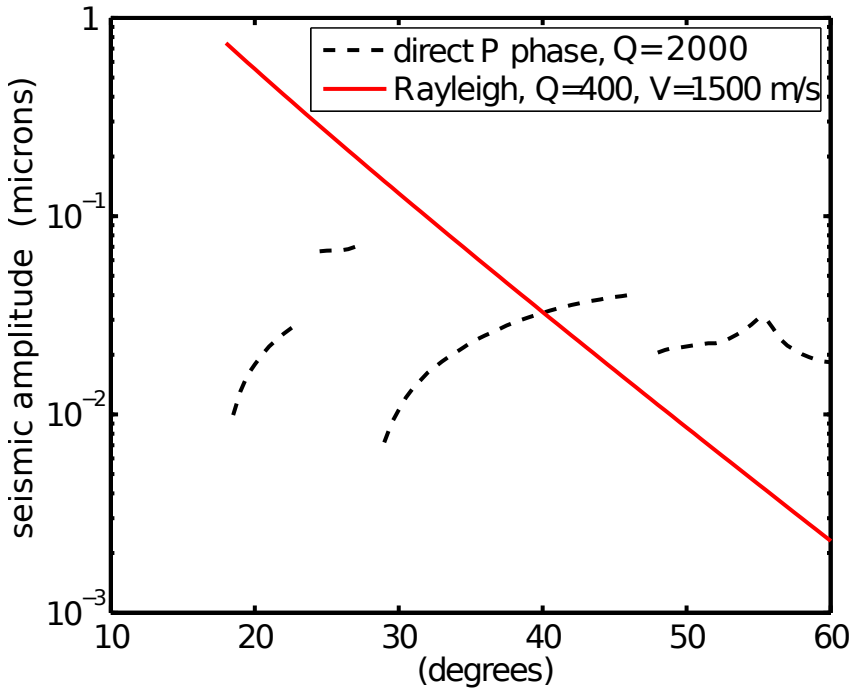

Figure 23.14: Estimates of the rms vertical ground displacement associated with Rayleigh or P waves, as a function of the epicentric angle Δ, for a source of intensity $\int F_{p2,\mathrm{surf}}(\mathbf{K}=0,f)\mathrm{d}f = 4.2\times10^4$ hPa^2 m^2 over a 330 by 330 km square, assuming an attenuation factor $Q = 2000$ for the P waves (Pasyanos et al., 2009), with travel times given by the ak135 reference Earth model (Snoke, 2009).

sum of propagating (acoustic, l real) and evanescent (acoustic-gravity, l imaginary) modes,

$$\phi_2 = \phi_{2,p} + \phi_{2,e}. \tag{23.95}$$

We get the frequency spectrum of the propagating modes by integrating over the inner regions of the wavenumber space (labelled P+S, S and R in figure 23.10),

$$F_{p2,p}(f_s) = \int_{K<\omega_s/\alpha_w} F_{p2,\mathrm{surf}}(\mathbf{K},f_s)\mathrm{d}\mathbf{K}. \tag{23.96}$$

For this range of wavenumbers $|k-k'| < K < \omega_s/\alpha_w$, and using the relations $\omega_s \simeq 4\pi f$ and, (for small $|f-f'|$), $|k-k'| \simeq 2\pi|f-f'|/C_g \simeq 8\pi^2 f|f-f'|$, we obtain an upper bound for the frequency difference $|f-f'| < g/(2\pi\alpha_w)$ which is close to= 0.001 Hz. Typical ocean wave spectra have a relative frequency half-width σ_f/f that is between 0.03 for swells and and 0.07 for wind-seas (Hasselmann et al., 1973), so that $E(f) \simeq E(f')$ is a good approximation for the interactions that drive long wavelength pressure fluctuations.

The wave spectrum is thus broad enough for us to evaluate $F_{p2,\mathrm{surf}}$ at $K = 0$ using eq. (23.22), and take it out of the integral in eq. (23.96). The acoustic spectrum simplifies to

$$F_{p2,p}(f_s) = \frac{\pi\omega_s^2}{\alpha_w^2}\rho_w^2 g^2 f_s E^2(f) I(f). \tag{23.97}$$

This is identical to the expression given by Lloyd (1981).

Gravity noise in an unbounded ocean

The pressure associated with acoustic-gravity modes is the other part of the integral in (23.96), for $K > \omega_s/\alpha_w$. The imaginary wave number l gives a vertical attenuation of the power spectrum by a factor $\mathrm{e}^{-2|l|z}$. With that attenuation we may, for large enough depths, assume that only modes with $K \ll k$ contribute to the result, so that we may take $F_{p2,\mathrm{surf}}(\mathbf{K},f_s) \simeq F_{p2,\mathrm{surf}}(\mathbf{K}=0,f_s)$, and take it out of the integrand. This approximation is valid only up to a maximum wave number $K_{\max}$ that is a small fraction of k, $K_{\max} = \epsilon k$. For numerical applications we used $\epsilon = 0.2$.

With this approximation we have,

$$\begin{aligned} F_{p2,e}(f_s,z) &= F_{p2,\mathrm{surf}}(\mathbf{K}=0,f_s)2\pi\int_{\omega_s/\alpha_w}^{K_{\max}} K\mathrm{e}^{2|l|z}\mathrm{d}K \\ &= F_{p2,\mathrm{surf}}(\mathbf{K}=0,f_s)2\pi\int_{0}^{K_{\max}} |l|\mathrm{e}^{2|l|z}\mathrm{d}|l| \\ &= \frac{\pi}{2z^2}\rho_w^2 g^2 f_s\left[1-\mathrm{e}^{2zK_{\max}}\right]E^2(f)I(f) \end{aligned} \tag{23.98}$$

A previous investigation by Cox and Jacobs (1989) included an extra factor $(1+zK_{\max})$ in front of the exponential term $\mathrm{e}^{2zK_{\max}}$, because they neglected compressibility effects. That term , however, is negligible in the upper part of the water column, and their observations collected within 100 to 290 m of the surface in 4000 m depth, are thus not affected by this small compressibility correction.

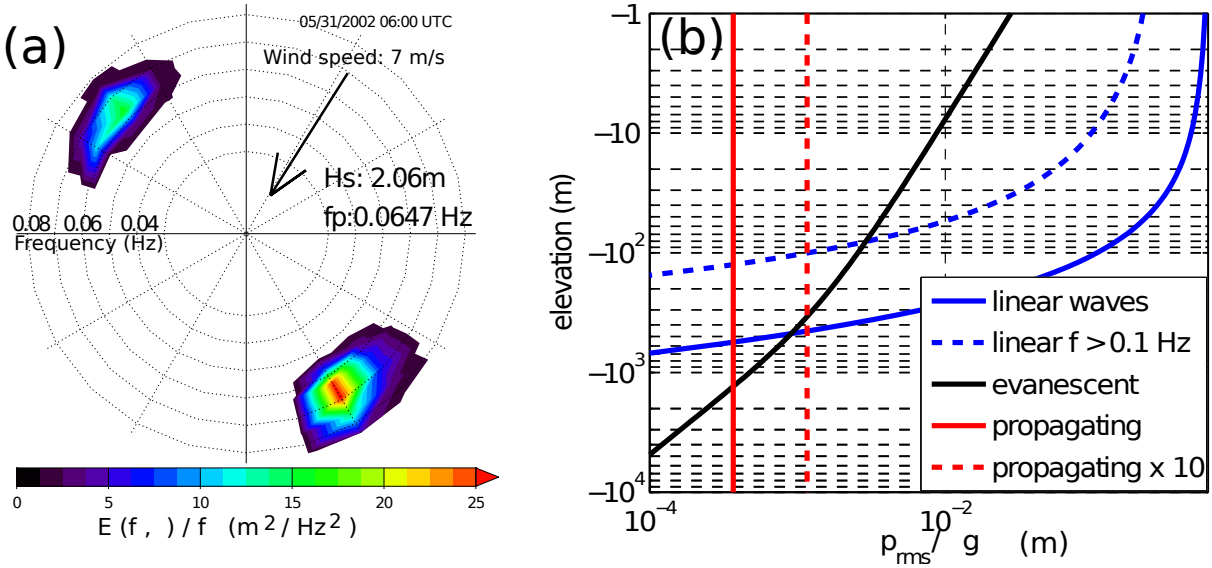

Figure 23.15: Example of (a) directional wave spectrum and (b) resulting profiles of the different contributions to the pressure fluctuations in the ocean, assuming infinite water depth. The ratio of double frequency to linear wave contributions depends on the amplitude of the waves and on the directional spectral shape, because all double frequency contributions are proportional to $E^2(f)I(f)$. This directional spectrum was estimated with a numerical wave model, and corresponds to the loudest noise event recorded at the ocean bottom seismometer H2O, on 31 May 2002 at 25 N, 136 W. This unusual spectrum has large wave energies in opposite directions, radiated from a North Pacific storm and Hurricane Alma (This event is analyzed in detail by Obrebski et al., 2012).

As shown in figure 23.15, the oceanic pressure signals can be dominated by linear gravity waves down to depths of a few hundred meters. When looking at the double frequency band, linear waves may only dominate in the top 100 m. At these frequencies, the acoustic-gravity modes have the most important contribution between about 100 to 500 m, provided that $E^2(f)I(f)$ is large enough. Propagating modes should dominate only beyond about 1000 m in the case of an unbounded ocean, or only 300 m, when accounting for the reverberation in a finite depth ocean, assuming a typical tenfold amplification for a sea floor with realistic elastic properties[2]. These depths will be reduced in the case of surface gravity waves with periods shorter than the 15 s swells example shown in figure 23.15.

Noise in a finite depth ocean

For large depths compared to the OSGW wavelength, $kh \gg 1$, the finite depth has little effect on the evanescent modes except for a doubling of the motion amplitude near the bottom, as the vertical profiles

[2]This amplification depends not only on the impedance ratio of the water and crust, which defines the amplification coefficients c_j derived below, but also on the seismic attenuation coefficient Q, which is discussed in section 4. Realistic calculations following Ardhuin et al. (2011) typically give a factor 10 to 20 amplification of the sound in the water column due to the bottom elasticity.

of the form $\exp(Kz)$ are replaced by $\cosh(Kz+Kh)/\cosh(Kh)$. This is similar to the finite depth effect on linear wave motions. However, the propagating modes radiated by the surface will now undergo multiple reflections at the bottom and sea surface, as shown in figure 23.5. The oceanic acoustic field is tightly coupled to elastic waves in the crust through these reflections.

One of the greatest complications induced by the presence of a bottom is the heterogeneity of the sediment and rock layers below the water column. The natural layering of the crust has a strong influence on the sound reflection and the nature of the seismic modes (e.g. Latham and Sutton, 1966; Abramovici, 1968).

23.5 Modeling of seismic spectra using a numerical wave model

While Hasselmann (1963) and Szelwis (1982) already made some order of magnitude estimates of the microseism generated by realistic wave spectra, the first attempt using a numerical wave model was performed by Kedar et al. (2008).

For a seismic frequency $f_s = 0.15$ Hz, the maximum of $\widetilde{C}$ corresponds to a depth $D \simeq 2300$ m. This explains why oceanic ridges are generally stronger sources of microseisms at that frequency (figure 23.16).

23.5.1 Rayleigh wave propagation in a non-homogeneous medium

Changes in water depth, as well as changes in sediment properties, have a large influence on the phase speeds and group speeds of seismic waves (figure 23.7). We thus expect that seismic waves are refracted and reflected. For $f_s = 0.15$ Hz Rayleigh waves typically speed up from phase speeds around $C_o = 2000$ m/s with a water depth of 3000 m to $C_c = 2570$m/s.

Besides, the amplitude of the vertical ground motion δ at the top of the crust is related to the energy flux. Without dissipation and neglecting reflections and lateral variations along direction y, the evolution of δ along the x direction between an ocean with a water depth h and the continent is given by

$$U(h_1)T_{E\delta}(h_1)\delta^2(h_1) = U(0)T_{E\delta}(0)\delta^2(0). \tag{23.99}$$

with $V(h_1)$ and $V(0)$ the group speeds over the ocean and over land, $T_{E\delta}(h_1)$ and $T_{E\delta}(0)$ being the transfer functions from the seismic energy to the vertical displacement at the top of the crust.

Hence, just like waves propagating from deep to shallow waters, the variance of the displacement $\delta^2/2$ is amplified by a factor $U(h_1)T_{E\delta}(h_1)/(V(0)T_{E\delta}(0))$ that can be of the order of 5 (figure 23.17). As a result, the 0 mode progressively transforms into a continental Rayleigh wave.

In the case of higher modes, they do not exist as such when the water depth goes below a critical value h_c. At these locations it is possible that they get transformed to mode 0. The real problem is made much more complex by the layering of sediments and rocks and their horizontal heterogeneity (Gualtieri et al., 2015).

23.5.2 Validation of modeled microseism

The microseism sources add up along their propagation and their amplitude is modified by dissipation, scattering and refraction. As a result, for a land-based station, nearby ocean sources have a stronger contributuon to the measured microseism than far away sources of equal power. Neglecting refraction effects, the only propagation effect taht we keep is the attenuation that we assume constant.

This gives a power spectral density of the vertical ground motion for an observation longitude λ and latitude ϕ that is the sum of sources over all oceans,

$$F_\delta(\lambda,\phi,f_s) = \int_{-\pi/2}^{\pi/2}\int_0^{2\pi} \frac{S_{DF}(f_s)}{R_E\sin\alpha}\, \mathrm{e}^{-2\pi f_s \alpha R_E/(VQ)}(R_E^2\sin\phi'\mathrm{d}\lambda'\mathrm{d}\phi')$$

where V is the seismic group speed, and Q is an attenuation factor. Taking $V = 1.8$ km s^{-1} and $Q = 150$, the energy of seismic waves with frequency $f_s = 0.15$ Hz is halved every 200 km. These two parameters are functions of the vertical structure and horizontal non-homogeneities of the Earth's crust. In particular Q may have large variations from about 100 to 1000, primarily increasing with the age of the crust.

For seismic stations located in France $Q \simeq 130$ gives a good agreement between model and observations for $f_s = 0.14$ Hz (figure 23.18.b), alors que pour certaines stations en Californie il faut reduire Q

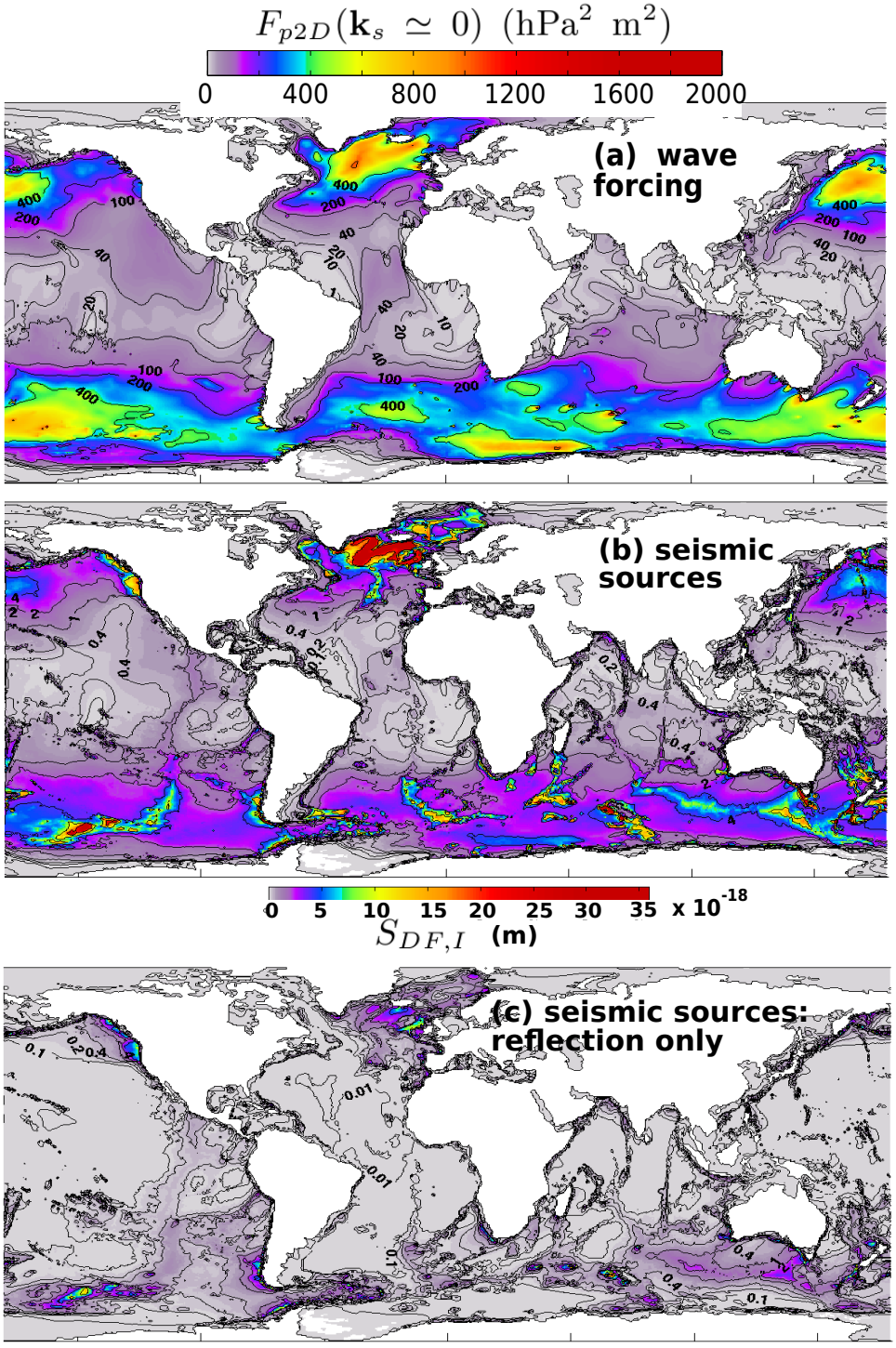

Figure 23.16: Averaged microseism sources averaged over the year 2008 at global scales over the seismic frequency band 0–0.34 Hz, based on a numerical wave model (Ardhuin et al., 2011). The top panel shows the average wave-induced pressure spectral density $F_{p2D}(k_x = 0, k_y = 0) = \int F_{p3D}(k_x = 0, k_y = 0, f_s)\mathrm{d}f_s$. The middle panel shows the seismic source, which combines the wave-induced pressure and the local amplification factor that varies with water depth $S_{DF}(f_s)$. The bottom panel shows the contribution of coastal reflections only given as the difference of the model run with reflection and the model run without reflection. For reference, without scattering or dissipation a constant source of 10×10^{-18} over a square with side length of 330 km gives an average amplitude $\delta^2_{\mathrm{rms}} = 1\mu\mathrm{m}^2$ at a distance of 1000 km.

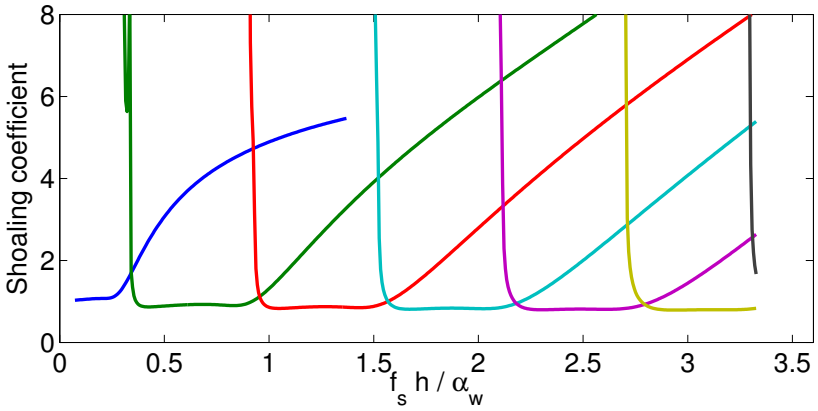

Figure 23.17: Amplification coefficient for the vertical displacement variance at the top of the crust, when Rayleigh waves propagate perpendicular to shore from ocean to land, as a function of the ocean depth.

to pres de 45 (figure 23.18.a). De faibles valeurs de Q impliquent que l'essentiel du bruit sismique vient de regions tres proches de la station de mesure, les sources plus lointaines ayant ete fortement attenuees. En Europe de l'ouest on estime que le bruit sismique est tout autant cause par les vagues qui passent sur la dorsale medio-Atlantique que par l'effet des reflections sur les coast Atlantiques. Les vagues en Mediterranee peuvent aussi be une source significative (figure 23.18.c).

Parce qu'il faut des vagues de same frequence mais de directions opposees pour generer du bruit sismique, les sources sont associees to des houles opposees la mer du vent, ou to la reflexion des vagues, to la coast ou par des icebergs. Avec un modele assez simple de la reflexion to la coast on peut simuler le bruit sismique de facon tres realiste. La principale inconnue etant l'attenuation des ondes sismiques lors de leur propagation.

La figure 23.19 montre la variation au cours de l'annee 2008 de l'amplitude du deplacement sismique vertical $\delta_{\rm rms}$ observe et modelise par l'equation (23.100) pour les stations SSB et BKS.

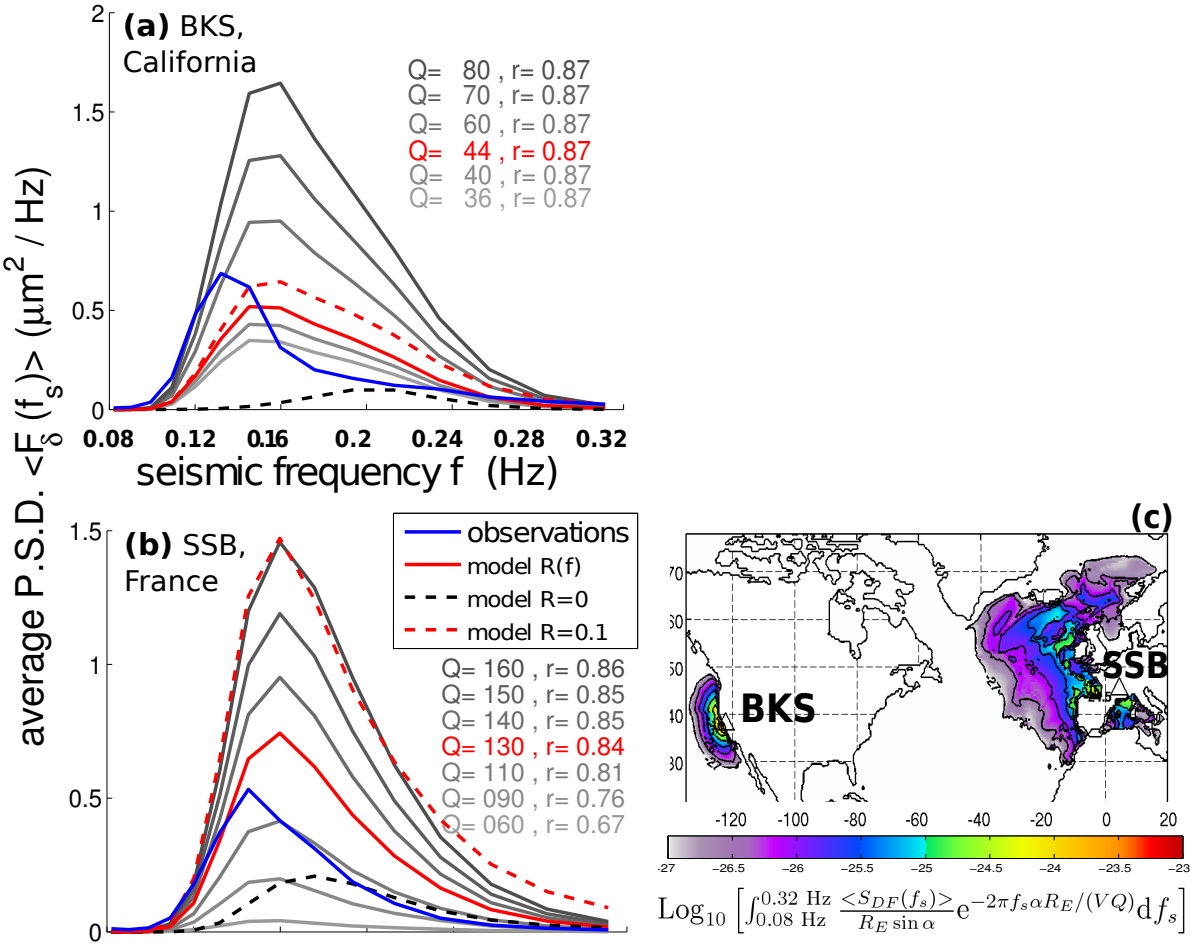

Figure 23.18: (a et b) spectres moyens du deplacement sismique observe et modelise avec differentes valeurs du facteur de qualite Q. Pour la valeur optimale de Q les resultat avec differentes modelisations de la reflection des vagues par la coast sont aussi montres: une reflexion constante de 10%, pas de reflexion du tout ($R = 0$) ou alors une reflection $R(f_s)$ variant lineairement avec la frequence. Dans le cas de SSB cette variation est de $R = 0.06$ pour $f_s = 0.04$ Hz to $R = 0.01$ at $f_s = 0.15$ Hz et pour BKS cette reflexion est augmentee de 50%. (c) Moyenne des contributions au bruit sismique pour l'annee 2008, pour les stations de Berkeley (BKS) et de Saint Sauveur en Rue (SSB), au sud de Saint-Etienne.

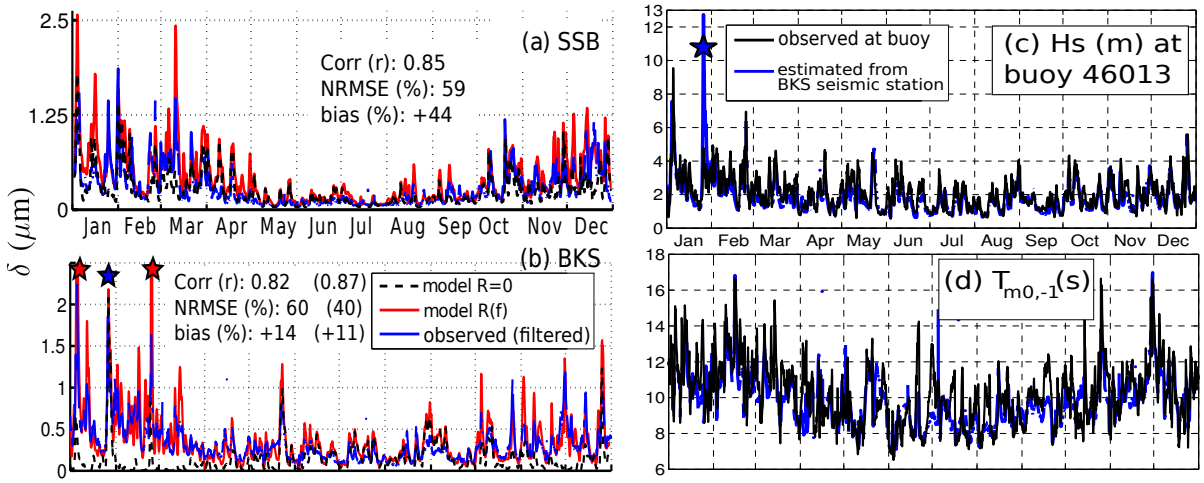

Figure 23.19: Relation entre signal sismique et houle coastal.
Series temporelles du deplacement sismique vertical $\delta_{\rm rms}$ observe et modelise par l'equation (23.100) pour les stations (a) SSB et (b) BKS. (c) et (d) En bas, serie temporelle de hauteurs significatives et periode moyenne des vagues mesurees to 46013 et reconstruite to partir du signal sismique to BKS.

Chapter 24

Microbaroms

Just like seismic motions contain a background of microseisms, atmospheric pressure also contains a backgroud od "microbaroms" that are radiated from ocean waves. However, this background is easily drowned in wind noise and is less visible than the microseism signal, and only in a narrow frequency window from 0.1 to 0.3 Hz. The first observations of microbaroms were made by Shuleikin (1935) over the black Sea and Benioff and Gutemberg (1939) on land. The first satisfactory theoretical explanation of microbarom generation for a homogeneous atmosphere was made by Brekhovskikh et al. (1973) following the theories for microseisms. A recent extension of the theory to an ocean of finite depth was given by De Carlo et al. (2020) with a verification against measurements by De Carlo et al. (2021), showing that it better fits observations than alternative or simplifiled theories. This recent numerical modelling of microbaroms still contain a number of empirical adjustments, and here we will sketch how a more complete theory could be given, considering microbarom generation in the presence of atmospheric wave guides, instead of adding the effects of wave guides after the fact. Indeed, the main atmospheric wave guides that are followed by microbaroms go through the stratosphere or the mesosphere. As a result, microbaroms are of particular interested as a possible source for upper atmosphere tomography (Donn and Rind, 1971; Smets and Evers, 2014) and the possiblity of detection of other signals in the 0.1 to 0.3 Hz band. More details about microbaroms can be found in Carlo (2020).

24.1 Microbarom generation: piston effect

The first qualitatively correct idea for the generation of microbaroms was formulated by Posmentier (1967), but it only strictly applies to vertically propagating acoustic waves. Here we use the generalization proposed by Ardhuin and Herbers (2013).

We may consider the atmospheric motion to be irrotational, so that the equations of motion are identical in the atmosphere and in an unbounded ocean, with the only difference that the atmospheric density is ρ_a and the atmospheric sound speed is α_a. We can thus use results from the previous chapter and first consider the solutions to the linearized acoustic equation eq. (23.12).

The second-order velocity potential takes the form,

$$\phi_{2,a} \propto \exp[\mathrm{i}(K_x x + K_y y + l_a z - \omega_s t)] \quad \text{for} \quad z > 0, \tag{24.1}$$

with

$$l_a = \sqrt{\frac{\omega_s^2}{\alpha_a^2} - K^2}. \tag{24.2}$$

Because $\rho_w/\rho_a \simeq 1000$, the air motion has only a small $O(\rho_w/\rho_a)$ local influence on the water motion, so that the solutions derived earlier for the water motion remain valid in the presence of air. The air motion, with a velocity potential ϕ_a also obeying eq. (23.12) is fully determined from the water motion via the kinematic boundary conditions on the air and water-sides of the interface (22.13),

$$\frac{\partial \phi_a}{\partial z} - \frac{\partial \phi}{\partial z} \simeq \boldsymbol{\nabla}\left(\phi_a - \phi\right) \cdot \boldsymbol{\nabla}\zeta - \zeta \frac{\partial^2 \left(\phi_a - \phi\right)}{\partial^2 z} \quad \text{at} \quad z = 0. \tag{24.3}$$

From the first order potential in the air (e.g. Waxler and Gilbert, 2006)

$$\phi_1 = \sum_{\mathbf{k},s} \mathrm{i}s \frac{g}{\sigma} Z^s_{1,\mathbf{k}} \mathrm{e}^{-kz} \mathrm{e}^{\mathrm{i}(\mathbf{k}\cdot\mathbf{x} - s\sigma)} \tag{24.4}$$

we obtain the second order potential,

$$\frac{\partial \phi_{2,a}}{\partial z} = \frac{\partial \phi_2}{\partial z} + \sum_{\mathbf{k},s,\mathbf{k}',s'} D_{za}\left(\mathbf{k},s,\mathbf{k}',s',z\right) Z^{s}_{1,\mathbf{k}} Z^{s'}_{1,\mathbf{k}'} \mathrm{e}^{\mathrm{i}\Theta(\mathbf{k},\mathbf{k}',s,s')}$$

and a new coupling coefficient

$$D_{za}\left(\mathbf{k},s,\mathbf{k}',s',z\right) = -\frac{2\mathrm{i}sg}{\sigma}\left(kk' + \mathbf{k}\cdot\mathbf{k}'\right). \tag{24.5}$$

We note that for $\mathbf{k}' = -\mathbf{k}$, $D_{za} = 0$, so that the long-wavelength motion with $K \ll k$ simplifies to

$$\frac{\partial \phi_{2a}}{\partial z} \simeq \frac{\partial \phi_2}{\partial z} \quad \text{at} \quad z = 0. \tag{24.6}$$

consistent with the result given by Posmentier (1967) for the interaction of monochromatic wave trains, and in disagreement with a factor 8 correction proposed by Arendt and Fritts (2000). This equation basically says that, at the surface, the vertical velocity in the air is equal to the vertical velocity in the water. In other words the surface is like a piston that transmits water motion to the air.

It all looks good except that, the vertical derivatives introduce the vertical wavenumbers in the air and in the water, so that the power spectrum of the atmospheric pressure is,

$$F_{p2,ap}(\mathbf{K},f_s) = \frac{\rho_a^2 \left|l^2\right|}{\rho_w^2 l_a^2} F_{p2,\mathrm{surf}}(\mathbf{K},f_s) \tag{24.7}$$

Which goes to infinity when l_a goes to zero, i.e. for horizontal propagation in the atmosphere that corresponds to a propagation angle in the water close to 12 degrees from the vertical. Clearly, some of our hypotheses do not apply as the atmospheric propagation angle goes to the horizontal. This problem was solved by Brekhovskikh et al. (1973), and it is explained in details by Carlo (2020). In fact the expression above here is good down to angles of 1° from the horizontal. In general we find

$$F_{p2,ap}(\mathbf{K},f_s) = \frac{\rho_a^2 R_a^2}{\rho_w^2} F_{p2,\mathrm{surf}}(\mathbf{K},f_s), \tag{24.8}$$

with R_a shown in Fig. 24.1. The ocean surface is thus a very strange piston that radiates most of the acoustic energy at angles close to the horizontal.

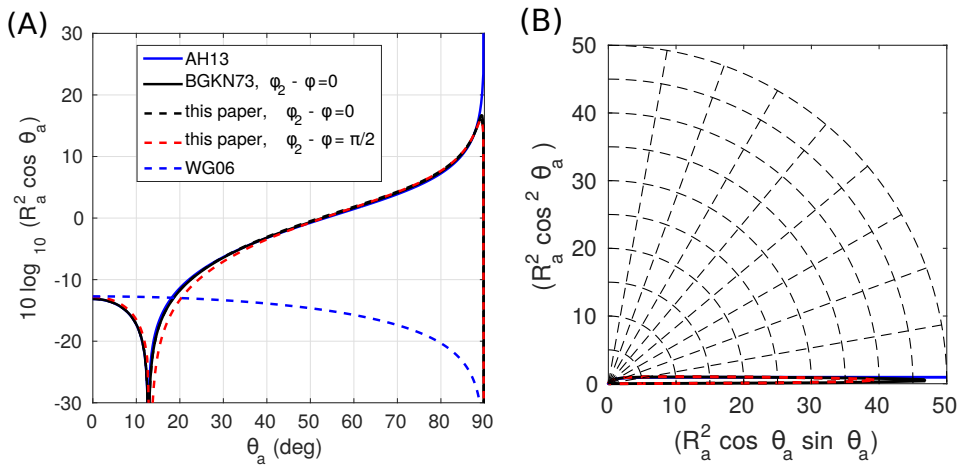

Figure 24.1: Radiation patterns for an ocean wave period of 10 s, given by the different theories without ocean bottom, in cartesian (A), and polar (B) representation, as a function of the acoustic propagation elevation angle θ_a (measured from the vertical). Note that when the radiated power is considered, these patterns must be multiplied by $\sin\theta_a$ before integration over θ_a. Reproduced from De Carlo et al. (2020).

For a quantitatively correct solution we have to keep all the terms in the equation, including the feedback of the atmospheric pressure on the ocean. For now, please go to chapter 3 of Carlo (2020). You may find more details here in the next version. In particular I may be brave enough to give you the microbarom source for a 2-layer or n-layer atmosphere to show how wave guides can be introduced in the theory without ad hoc handwaving.

Bibliography

Abramovici, F., 1968: Diagnostic diagrams and transfer functions for oceanic wave-guides. *Bull. Seism. Soc. Am.*, **58**, 426–456.

Algué, J., 1900: Relation entre quelques mouvements microséismiques et l'existence, la position et la distance des cyclones à Manille (Philippines). *Congrès international de Météorlogie, Paris*, 131–136.

Ardhuin, F., L. Gualtieri, and E. Stutzmann, 2015: How ocean waves rock the earth: two mechanisms explain seismic noise with periods 3 to 300 s. *Geophys. Res. Lett.*, **42**, 765–772. doi:10.1002/2014GL062782.

— 2019: Physics of ambient noise generation by ocean waves. *Ambient seismic noise*, N. Nakata, L. Gualtieri, and A. Fichtner, eds., Cambridge University Press, 69–107.

Ardhuin, F. and T. H. C. Herbers, 2013: Noise generation in the solid earth, oceans and atmosphere, from nonlinear interacting surface gravity waves in finite depth. *J. Fluid Mech.*, **716**, 316–348. doi:10.1017/jfm.2012.548.

Ardhuin, F., N. Rascle, and K. A. Belibassakis, 2008: Explicit wave-averaged primitive equations using a generalized Lagrangian mean. *Ocean Modelling*, **20**, 35–60. doi:10.1016/j.ocemod.2007.07.001.

Ardhuin, F., E. Stutzmann, M. Schimmel, and A. Mangeney, 2011: Ocean wave sources of seismic noise. *J. Geophys. Res.*, **116**, C09004.URL link. doi:10.1029/2011JC006952.

Arendt, S. and D. C. Fritts, 2000: Acoustic radiation by ocean surface waves. *J. Fluid Mech.*, **415**, 1–21.

Barrick, D. E. and B. L. Weber, 1977: On the nonlinear theory for gravity waves on the ocean's surface. Part II: Interpretation and applications. *J. Phys. Oceanogr.*, **7**, 3–10.URL link.

Benioff, H. and B. Gutemberg, 1939: Waves anc currents recorded by electromagnetic barographs. *Bull. Seismol. Soc. Am.*, **20**, 421–426. doi:10.1175/1520-0477-20.10.421.

Benjamin, T. B. and J. E. Feir, 1967: The disintegration of wav trains on deep water. part 1. theory. *J. Fluid Mech.*, **27**, 417–430.

Bertelli, T., 1872: Osservazioni sui piccoli movimenti dei pendoli in relazione ad alcuni fenomeni meteorologiche. *Boll. Meteorol. Osserv. Coll. Roma*, **9**, 10.

Biesel, F., 1952: Equations générales au second ordre de la houle irrégulière. *Houille Blanche*, **5**, 372–376.

Brekhovskikh, L. M., V. V. Goncharov, V. M. Kurtepov, and K. A. Naugolnykh, 1973: The radiation of infrasound into the atmosphere by surface waves in the ocean. *Izv. Atmos. Ocean. Phys.*, **9**, 899–907 (In the English translation, 511–515.).

Broche, P., J. C. de Maistre, and P. Forget, 1983: Mesure par radar décamétrique cohérent des courants superficiels engendrés par le vent. *Oceanol. Acta*, **6**, 43–53.

Carlo, M. D., 2020: *Characterization of atmospheric ambient noise from oceanic sources: globla modelling of microbaroms and verification with International Monitoring System infrasound data*. Ph.D. thesis, Université de Bretagne Occidentale, Brest, France.URL link.

Chalikov, D., 2007: Numerical simulation of the Benjamin-Feir instability and its consequences. *Phys. of Fluids*, **19**, 016602.

Cokelet, E. D., 1977: Steep gravity waves in water of arbitrary uniform depth. *Proc. Roy. Soc. Lond. A*, **286**, 183–230.

Cooper, R. I. B. and M. S. Longuet-Higgins, 1951: An experimental study of the pressure variations in standing water waves. *Proc. Roy. Soc. Lond. A*, **206**, 426–435. doi:10.1098/rspa.1951.0079.

Cox, C. S. and D. C. Jacobs, 1989: Cartesian diver observations of double frequency pressure fluctuations in the upper levels of the ocean. *Geophys. Res. Lett.*, **16**, 807–810.

Creamer, D. B., F. Henyey, R. Schult, and J. Wright, 1989: Improved linear representation of ocean surface waves. *J. Fluid Mech.*, **205**, 135–161.

Dalrymple, R. A., 1974: A finite amplitude wave on a linear shear current. *J. Geophys. Res.*, **79**, 4498–4504. doi:10.1029/jc079i030p04498.

De, S. C., 1955: Contributions to the theory of Stokes waves. *Proceedings of the Cambridge philosophical*

society, **51**, 713–736.

De Carlo, M., F. Ardhuin, and A. L. Pichon, 2020: Atmospheric infrasound radiation from ocean waves in finite depth: a unified generation theory and application to radiation patterns. *Geophys. J. Int.*, **221**, 569–585. doi:10.1093/gji/ggaa015.

De Carlo, M., P. Hupe, A. Le Pichon, and F. Ardhuin, 2021: Global microbarom patterns: a first confirmation of the theory for source and propagation. *Geophys. Res. Lett.*, **48**, e2020GL090163. doi:10.1029/2020GL090163.

Dean, R. G., 1965: Stream function representation of nonlinear ocean waves. *J. Geophys. Res.*, **70**, 4561–4572.

Dean, R. G. and R. A. Dalrymple, 1991: *Water wave mechanics for engineers and scientists*. World Scientific, Singapore, second edition, 353 pp.

Donn, W. L. and D. Rind, 1971: Natural infrasound as an atmospheric probe. *Geophys. J. R. Astron. Soc.*, **26**, 111–133. doi:10.1111/j.1365-246x.1971.tb03386.x.

Farra, V., E. Stutzmann, L. Gualtieri, M. Schimmel, and F. Ardhuin, 2016: Ray-theoretical modeling of secondary microseism P-waves. *Geophys. J. Int.*, **206**, 1730–1739. doi:10.1093/gji/ggw242.

Farrell, W. E. and W. Munk, 2008: What do deep sea pressure fluctuations tell about short surface waves? *Geophys. Res. Lett.*, **35**, L19605. doi:10.1029/2008GL035008.

Fermi, E., J. Pasta, and S. Ulam, 1955: Studies of nonlinear problems. i. *Nonlinear wave motion. Lectures in applied mathematics, vol. 15*, A. C. Newell, ed., Amer. Math. Soc., Providence, R.I., pages 143–156.

Gualtieri, L., E. Stutzmann, Y. Capdeville, F. Ardhuin, M. Schimmel, A. Mangeney, and A. Morelli, 2013: Modelling secondary microseismic noise by normal mode summation. *Geophys. J. Int.*, **193**, 1732–1745. doi:10.1093/gji/ggt090.

Gualtieri, L., E. Stutzmann, Y. Capdeville, V. Farra, A. Mangeney, and A. Morelli, 2015: On the shaping factors of the secondary microseismic wavefield. *J. Geophys. Res.*, **120**, 1–22. doi:10.1002/2015JB012157.

Gualtieri, L., E. Stutzmann, V. Farra, Y. Capdeville, M. Schimmel, F. Ardhuin, and A. Morelli, 2014: Modelling the ocean site effect on seismic noise body waves. *Geophys. J. Int.*, **193**, 1096–1106. doi:10.1093/gji/ggu042.

Hasselmann, K., 1960: Grundgleichugen der seegangsvorhersage. *Schifftechnik*, **7**, 191–195.

— 1962: On the non-linear energy transfer in a gravity wave spectrum, part 1: general theory. *J. Fluid Mech.*, **12**, 481–501.

— 1963: A statistical analysis of the generation of microseisms. *Rev. of Geophys.*, **1**, 177–210.

— 1966: Feynman diagrams and interaction rules of wave-wave scattering processes. *Rev. of Geophys.*, **4**, 1–32.

Hasselmann, K., T. P. Barnett, E. Bouws, H. Carlson, D. E. Cartwright, K. Enke, J. A. Ewing, H. Gienapp, D. E. Hasselmann, P. Kruseman, A. Meerburg, P. Müller, D. J. Olbers, K. Richter, W. Sell, and H. Walden, 1973: Measurements of wind-wave growth and swell decay during the Joint North Sea Wave Project. *Deut. Hydrogr. Z.*, **8**, 1–95, suppl. A.

Herbers, T. H. C. and R. T. Guza, 1991: Wind-wave nonlinearity observed at the sea floor. part I: forced-wave energy. *J. Phys. Oceanogr.*, **21**, 1740–1761.URL link.

Janssen, P. A. E. M., 2009: On some consequences of the canonical transformation in the Hamiltonian theory of water waves. *J. Fluid Mech.*, **637**, 1–44.

Janssen, P. A. E. M. and M. Onorato, 2007: The intermediate water depth limit of the Zakharov equation and consequences for wave prediction. *J. Phys. Oceanogr.*, **37**, 2389–2400. doi:10.1175/JPO3128.1.

Kedar, S., M. Longuet-Higgins, F. W. N. Graham, R. Clayton, and C. Jones, 2008: The origin of deep ocean microseisms in the north Atlantic ocean. *Proc. Roy. Soc. Lond. A*, 1–35. doi:10.1098/rspa.2007.0277.

Kirby, J. T., 1998: Discussion of 'note on a nonlinearity parameter of surface waves' by S. Beji. *Coastal Eng.*, **34**, 163–168.

Krasitskii, V. P., 1994: On reduced equations in the Hamiltonian theory of weakly nonlinear surface waves. *J. Fluid Mech.*, **272**, 1–20.

Lamb, H., 1932: *Hydrodynamics*. Cambridge University Press, Cambridge, England, 6th edition, 738 pp.

Latham, G. V. and G. H. Sutton, 1966: Seismic measurements on the ocean floor. *J. Geophys. Res.*, **71**, 2545–2573.

Lay, T. and T. C. Wallace, 1995: *Modern Global Seismology*. Academic Press, San Diego, CA, 517 pp., iSBN 0-12-732870-X.

Levi-Civita, T., 1925: Détermination rigoureuse des ondes permanentes d'ampleur finie. *Matematische Annalen*, **XCII**, 264–314.

Lighthill, J., 1978: *Waves in fluids*. Cambridge University Press, Cambridge, United Kingdom, 504 p.

Lloyd, S. P., 1981: Underwater sound from surface waves according to the Lighthill-Ribner theory. *J. Acoust. Soc. Amer.*, **69**, 425–435.

Longuet-Higgins, M. S., 1950: A theory of the origin of microseisms. *Phil. Trans. Roy. Soc. London A*, **243**, 1–35.

Longuet-Higgins, M. S. and J. D. Fenton, 1974: On the mass, momentum, energy and circulation of a solitary wave. II. *Proc. Roy. Soc. Lond. A*, **340**, 471–493.

Longuet-Higgins, M. S. and O. M. Phillips, 1962: Phase velocity effects in tertiary wave interactions. *J. Fluid Mech.*, **12**, 333–336.

Miche, A., 1944: Mouvements ondulatoires de la mer en profondeur croissante ou décroissante. Première partie. Mouvements ondulatoires périodiques et cylindriques en profondeur constante. *Annales des Ponts et Chaussées*, **Tome 114**, 42–78.

Miller, G. F. and H. Pursey, 1955: On the partition of energy between elastic waves in a semi-infinite solid. *Proc. Roy. Soc. Lond. A*, **233**, 55–69.

Nishida, K. and R. Takagi, 2016: Teleseismic S wave microseisms. *Science*, **353**, 919–921. doi:10.1126/science.aaf7573.

Obrebski, M., F. Ardhuin, E. Stutzmann, and M. Schimmel, 2012: How moderate sea states can generate loud seismic noise in the deep ocean. *Geophys. Res. Lett.*, **39**, L11601. doi:10.1029/2012GL051896.

— 2013: Detection of microseismic compressional (p) body waves aided by numerical modeling of oceanic noise sources. *J. Geophys. Res.*, **118**, 4312–4324. doi:10.1002/jgrb.50233.

Pasyanos, M. E., W. R. Walter, and E. M. Matzel, 2009: A simultaneous multiphase approach to determine p-wave and s-wave attenuation of the crust and upper mantle. *Bull. Seismol. Soc. Am.*, **99**, 3314–3325.

Posmentier, E., 1967: A theory of microbaroms. *Geophys. J. R. Astron. Soc.*, **13**, 487–501.

Prevosto, M. and G. Z. Forristall, 2002: Statistics of wave crest from models vs. measurements. *Proceedings of OMAE 2002 21st International Conference on Offshore Mechanics and Arctic Engineering, 23-28 June 2002, Oslo, Norway*, ASME, OMAE2002–28446.

Schwartz, L. W., 1974: Computer extension and analytic continuation of Stokes' expansion for gravity waves. *J. Fluid Mech.*, **62**, 553–578.

Shapiro, N. M., M. Campillo, L. Stehly, and M. H. Ritzwoller, 2005: High-resolution surface-wave tomography from ambient seismic noise. *Science*, **307**, 1615–1617. doi:10.1111/j.1365-246X.2006.03240.x.

Shuleikin, V. V., 1935: The voice of the sea. *Dokl. Akad. Nauk SSSR*, **3**, 259.

Smets, P. S. M. and L. G. Evers, 2014: The life cycle of a sudden stratospheric warming from infrasonic ambient noise observations. *J. Geophys. Res.*, **119**, 12,084–12,099. doi:10.1002/2014JD021905.

Snoke, J. A., 2009: Traveltime tables for iasp91 and ak135. *Seismological Research Letters*, **88**, 260–262.

Stokes, G. G., 1880: On the theory of oscillatory waves, appendix B. *Math. and Phys. papers*, Cambridge University Press, volume 1, 225–2228.

Stoneley, R., 1926: The effect of the ocean on Rayleigh waves. *Mon. Not. Roy. Astron. Soc.*, **Geophys. Suppl. 1**, 349–356.

Stutzmann, E., G. Roult, and L. Astiz, 2000: Geoscope station noise level. *Bull. Seismol. Soc. Am.*, **90**, 690–701.

Szelwis, R., 1982: Modeling of microseismic surface wave source. *J. Geophys. Res.*, **87**, 6906–6918.

Ursell, F., 1953: The long-wave paradox in the theory of gravity waves. *Proceedings of the Cambridge philosophical society*, **49**, 685–694.

Vinnik, L. P., 1973: Sources of microseismic P waves. *Pure Appl. Geophys.*, **103**, 282–289.

Waxler, R. and K. E. Gilbert, 2006: The radiation of atmospheric microbaroms by ocean waves. *J. Acoust. Soc. Amer.*, **119**, 2651–2664.

Webb, S. C., 2007: The earth's 'hum' is driven by ocean waves over the continental shelves. *Nature*, **445**, 754–756. doi:10.1038/nature05536.

Weber, B. L. and D. E. Barrick, 1977: On the nonlinear theory for gravity waves on the ocean's surface. Part I: Derivations. *J. Phys. Oceanogr.*, **7**, 3–10.URL link.

Zhang, J., P. Gerstoft, and P. D. Bromirski, 2010: Pelagic and coastal sources of P-wave microseisms: Generation under tropical cyclones. *Geophys. Res. Lett.*, **37**, L15301. doi:10.1029/2010GL044288.

Zopf, D. O., H. C. Creech, and W. H. Quinn, 1976: The wavemeter: a land-based system for measuring nearshore ocean waves. *Mar. Tech. Soc. Journal*, **10**, 19–25.